Slc6a4 silencing alleviates ropivacaine-induced injury in myocardial infarction cell models

Jing Wan*, Xiaonan Du, Peiwen Luo, Shenghua Li*

Department of Anesthesiology, The Central Hospital of Wuhan, Tongji Medical College, Huazhong University of Science and Technology, Wuhan City, Hubei Province, China

Submitted: 7 November 2024; **Accepted:** 9 December 2025
Online publication: 20 January 2026

Arch Med Sci
DOI: https://doi.org/10.5114/aoms/211891

***Corresponding authors:**
Shenghua Li, MD
Jing Wan
Department of Anesthesiology
The Central Hospital of Wuhan
Tongji Medical College
Huazhong University of Science and Technology
No. 26, Shengli Street
Jiang'an District
Wuhan City
Hubei Province
China, 430014
E-mail: Shli001@hotmail.com, wj075@hotmail.com

Abstract

Introduction: Myocardial infarction (MI), often caused by atherosclerotic plaque rupture, leads to severe myocardial ischemia and necrosis. Despite advancements in treatment, its molecular mechanisms remain incompletely understood. Local anesthetics such as ropivacaine, while beneficial for pain control, may induce cardiotoxicity, complicating MI management. This study aimed to explore the effects of ropivacaine on H9c2 cardiomyocytes and the protective potential of *Slc6a4* silencing against ropivacaine-induced cellular damage.

Material and methods: Bioinformatics analysis of the GSE97320 dataset identified MI-associated differentially expressed genes (DEGs), which overlapped with ropivacaine-related genes. H9c2 cells were cultured and treated with ropivacaine to induce myocardial injury. The effects on cell cycle, apoptosis, and oxidative stress were assessed, and the role of *Slc6a4* silencing under hypoxia/reoxygenation (H/R) conditions was investigated.

Results: Ropivacaine induced G1 phase arrest and apoptosis in H9c2 cells, with increased Bax and caspase-3 levels and decreased Bcl-2. Oxidative stress was elevated, as evidenced by increased ROS, MDA, and LDH levels and reduced SOD, GSH, and ATP. *Slc6a4* silencing under H/R conditions mitigated these effects, reducing cell cycle dysregulation and apoptosis by 40%, lowering NLRP3 inflammasome expression, and promoting Nrf2 nuclear translocation.

Conclusions: This study demonstrates that *Slc6a4* silencing alleviates ropivacaine-induced cellular damage by modulating oxidative stress, apoptosis, and cell cycle dynamics, suggesting a potential therapeutic strategy for myocardial ischemia-reperfusion injury.

Key words: *Slc6a4*, ropivacaine, myocardial infarction, oxidative stress, cell injury.

Introduction

Myocardial infarction (MI), commonly known as a heart attack, is a major cause of mortality and disability worldwide. It results from the obstruction of coronary blood flow, usually due to atherosclerotic plaque rupture and thrombosis, leading to ischemia and death of cardiomyocytes [1–3]. Traditional risk factors such as hypertension, diabetes, and smoking accelerate atherosclerosis and contribute to plaque instability [4, 5]. Recent studies have shown that excessive inflammation activation is an important driving factor of cardiovascular disease (CVD), which can

exacerbate cardiovascular injury and poor prognosis through pro-inflammatory cytokines and novel biomarkers (such as microRNA, ST2 protein, and adiponectin) [6].

Patients with type 2 diabetes mellitus (T2DM) or prediabetes (PDM) exhibit heightened inflammatory activity and oxidative stress, which exacerbate atherosclerosis and increase the likelihood of adverse cardiovascular events [7–9]. Despite significant progress in reperfusion strategies and pharmacotherapy, outcomes after MI remain heterogeneous, highlighting the need for novel therapeutic targets [6, 10].

Local anesthetics play an essential role in perioperative analgesia for cardiovascular patients. Ropivacaine, a long-acting amino amide anesthetic, is widely used due to its lower neurotoxicity and cardiotoxicity compared with bupivacaine [11, 12]. However, accumulating evidence indicates that ropivacaine exerts dose-dependent cardiotoxic effects, including impaired myocardial contractility, arrhythmias, and even myocardial depression [13, 14]. These risks are particularly concerning in the setting of ischemia/reperfusion injury, where the myocardium is already highly susceptible to further damage [15]. Therefore, elucidating the molecular mechanisms underlying ropivacaine-induced cardiotoxicity is of great importance for improving its clinical safety in MI patients.

The serotonin transporter gene (*SLC6A4*), which encodes the serotonin transporter (*5-HTT*), has traditionally been studied in the context of psychiatric disorders due to its key role in serotonin reuptake [16, 17]. However, emerging evidence also implicates *Slc6a4* in cardiovascular pathophysiology. Genetic variations and altered expression of SLC6A4 have been associated with MI risk, age of onset, and responses to myocardial injury [18–20]. Notably, *Slc6a4* expression was reported to be significantly downregulated following acute myocardial ischemia, suggesting a potential protective role in cardiomyocytes [21]. Yet, its contribution to ropivacaine-induced cardiotoxicity and myocardial ischemia/reperfusion injury (MIRI) remains poorly understood.

In this study, we integrated bioinformatics analysis of the GSE97320 dataset with experimental validation in H9c2 cardiomyocytes under hypoxia/reoxygenation (H/R) conditions. We specifically investigated whether *Slc6a4* silencing could attenuate ropivacaine-induced injury and explored its role in regulating oxidative stress, apoptosis, and cell cycle dynamics. By uncovering the interplay between *Slc6a4* and ropivacaine-induced cardiotoxicity, our findings aim to provide novel insights into therapeutic strategies for protecting the myocardium in MI patients. By combining transcriptomic data with functional experiments, this work provides new insights into the potential involvement of *Slc6a4* in ropivacaine-induced cardiotoxicity and suggests possible avenues for therapeutic exploration in MI patients.

Material and methods

Download of GSE97320 microarray dataset and screening of differentially expressed genes (DEGs)

The GSE97320 microarray dataset was obtained from the Gene Expression Omnibus (GEO) database (https://www.ncbi.nlm.nih.gov/gds/). It included gene expression profiles from three patients with acute MI and three healthy controls. Data preprocessing and differential expression analysis were performed using the R package "limma" (version 4.2.3). DEGs between the MI group and the control group were identified by thresholds of fold change (FC) > 1.3 for up-regulated genes and < 0.77 for down-regulated genes. The adjusted *p*-value (Benjamini-Hochberg correction) was < 0.05. This threshold was selected based on the methodology of Martínez-Martínez *et al*., who used similar criteria (FC > 1.3 or < 0.77) to detect differentially expressed proteins in myocardial fibrosis studies [22]. They emphasized that modest expression changes may have biological significance, especially in complex pathological conditions such as myocardial remodeling and extracellular matrix accumulation.

Identification and expression analysis of overlapping genes

To explore the potential molecular link between ropivacaine exposure and MI, we first retrieved a list of ropivacaine-related genes from the PubChem database (https://pubchem.ncbi.nlm.nih.gov/), which resulted in the identification of 29 candidate genes (Supplementary Table SI). DEGs obtained from the GSE97320 dataset were categorized into up-regulated and down-regulated gene sets based on defined fold changes and adjusted *p*-value thresholds. Subsequently, we performed a Venn diagram cross-tabulation analysis between the set of ropivacaine-associated genes and DEGs using the Sangerbox platform (version 3.0, http://vip.sangerbox.com/home.html) to identify overlapping genes that may represent potential ropivacaine-responsive targets in MI. We further analyzed these overlapping genes in the GSE97320 dataset to compare their expression profiles between MI patients and healthy controls.

Cell lines and culture

The H9c2 rat cardiomyoblast cell line was obtained from the American Type Culture Conser-

vation Center (ATCC, USA), and the cells were cultured in high-sugar Dulbecco's Modified Eagle Medium (DMEM; Gibco, USA) supplemented with 10% fetal bovine serum (FBS; Gibco, USA) to provide the nutrients, growth factors and hormones required for cell proliferation and survival. To prevent microbial contamination, the medium was supplemented with 1% penicillin-streptomycin solution (Gibco, USA), which has a broad-spectrum antimicrobial effect against both Gram-positive and Gram-negative bacteria. All cell cultures were incubated at 37°C in a humidified environment containing 5% CO_2. The medium was changed every 48 h, and cells were subcultured at 70–80% confluence using 0.25% trypsin-EDTA (Gibco, USA). All experiments were performed using cells in the logarithmic growth phase, and the experimental procedures were carried out under aseptic conditions in a Class II biosafety cabinet to ensure the consistency and sterility of the experiments. Cell grouping was achieved by randomly assigning culture wells to each treatment group using a random number table, in order to minimize batch effects. Given that all results were objective instrument readings, blinding was not implemented; however, data collection and analysis were independently repeated and cross-verified by two researchers to ensure objectivity.

Cell treatment and transfection

H9c2 cells were inoculated in 6-well plates at a density of 4×10^5 cells per well and incubated overnight at 37°C, 5% CO_2 to induce cell attachment. Cells were subsequently treated with ropivacaine hydrochloride (Sigma-Aldrich, USA) at final concentrations of 0.5 mM, 1 mM, and 2 mM for 24 h to induce a cytotoxic response. This treatment concentration range was referenced to the setting in the study of Zeng *et al*. This dose interval was confirmed to be effective in inducing apoptosis and a toxic response [23]. To knock down *Slc6a4* gene expression, H9c2 cells were inoculated in 24-well plates at a density of 2×10^5 cells per well and cultured to 70–80% fusion for transient transfection. Lipofectamine 3000 transfection reagent (Invitrogen, USA) was used according to the instructions, and the final concentration of *Slc6a4*-specific siRNA was 80 nM. A nontargeting scrambled siRNA was used as a negative control, and transfection efficiency was verified by qRT-PCR or Western blot (WB) after transfection. All treatments were set up in triplicate wells to ensure reproducibility.

Flow cytometry analysis of apoptosis and cell cycle

H9c2 cells, with approximately 80% confluence, were collected using 0.25% trypsin-EDTA (Gibco, USA) and then washed twice with ice-cold phosphate-buffered saline (PBS, pH 7.4) [24] to remove residual serum and enzymes. To detect apoptosis, cells were stained with annexin V-FITC and propidium iodide (PI) according to the manufacturer's instructions (BD Biosciences, USA). Cells were incubated in the dark for 15 min at room temperature, and 400 µl of binding buffer was added before analysis. For cell cycle analysis, cells were fixed in 70% ice-cold ethanol at –20°C overnight. After fixation, cells were rinsed with PBS and incubated with RNase A for 30 min at 37°C to remove RNA. They were then stained with PI for 30 min in the dark. All samples were analyzed using a BD LSRFortessa flow cytometer (BD Biosciences, USA), and data were processed using FlowJo v10 software (FlowJo LLC, USA). In apoptosis analysis, early apoptotic (annexin V^+/PI^-), late apoptotic (annexin V^+/PI^+), and necrotic (annexin V^-/PI^+) cell populations were quantified. In cell cycle analysis, the proportion of cells in G0/G1, S, and G2/M phases was calculated based on PI fluorescence intensity. Each experimental group was analyzed in triplicate to ensure reproducibility and statistical validity.

Quantitative real-time polymerase chain reaction (qRT-PCR)

The total RNA from H9c2 cells was extracted using TRIzol reagent (Thermo Fisher Scientific, USA) according to the manufacturer's instructions [25]. Complementary DNA (cDNA) was synthesized from 1 µg of total RNA using a PrimeScript RT kit (Takara, Japan) according to the manufacturer's instructions [26]. qRT-PCR was performed using the StepOnePlus Real-Time PCR System (Applied Biosystems, USA) and SYBR Green PCR Master Mix (Applied Biosystems, USA) [27]. Gene expression levels of *Cdkn1a* (p21), *Ccne1* (cyclin E), *Cdk4*, *Bax*, *Bcl2*, *Casp3*, *Slc6a4*, *Pcsk2*, *Pomc*, *Il18*, and *Il1b* were quantified. The expression levels of all target genes were normalized to *Gapdh* from the same sample and calculated using the $2^{-\Delta\Delta Ct}$ method; a no-template control was included on each plate, and a ΔCt of *Gapdh* < 0.5 was considered valid [28]. The set of primer sequences is shown in Table I.

Western blot (WB) assay

Total protein from H9c2 cells was extracted using radioimmunoprecipitation assay (RIPA) lysis buffer (Thermo Fisher Scientific, USA), and a protease and phosphatase inhibitor cocktail (Thermo Fisher Scientific, USA) was added to prevent protein degradation [29]. Supernatants containing total protein were collected, and protein concentrations were quantified using a bicinchoninic acid (BCA) protein assay kit (Thermo Fisher Sci-

Table I. Primer sequences for qRT-PCR.

Target	Direction	Sequence (5′–3′)
Pcsk2	Forward	AAAATACCACCCACCGGCAA
Pcsk2	Reverse	CGAGGTAGCGGACGAAGTTT
Pomc	Forward	GCCACTGAACATCTTCGTCCT
Pomc	Reverse	CTGAGGCTCTGTCGCGGAA
Slc6a4	Forward	TCCTCCGCTTTGGCGCCTCTTCC
Slc6a4	Reverse	TGGGGGTTGCAGGGGAGATCCTG
Cdkn1a (p21)	Forward	CTGGATGCTAGAGGTCTGC
Cdkn1a (p21)	Reverse	AGAGTTGTCAGTGTAGATGC
Ccne1 (Cyclin E1)	Forward	TTTGCAAGATCCGGATGAA
Ccne1 (Cyclin E1)	Reverse	CGCTGAATCATCATCCCAAG
Cdk4	Forward	AGTCAGTGGTGCCGGAGATG
Cdk4	Reverse	CAGCGTCCGGAAACTGGAA
Bax	Forward	CGGCGAATTGGAGATGAACTGG
Bax	Reverse	CTAGCAAAGTAGAAGAGGGCAACC
Bcl2	Forward	TGTGGATGACTGACTACCTGAACC
Bcl2	Reverse	CAGCCAGGAGAAATCAAACAGAGG
Casp3	Forward	GTGGAACTGACGATGATATGGC
Casp3	Reverse	CGCAAAGTGACTGGATGAACC
Il18	Forward	CAGCTCTTCTACCAGCAAACAT
Il18	Reverse	GCTGTGTTGTAAGGAGAGTGC
Il1b	Forward	CCTATGTCTTGCCCGTGGAG
Il1b	Reverse	CACACACTAGCAGGTCGTCA
Gapdh	Forward	TGCCACTCAGAAGACTGTGG
Gapdh	Reverse	GGATGCAGGGATGATGTTCT

entific, USA) according to the manufacturer's instructions [30]. Aliquots of proteins were mixed with SDS sample upload buffer, denatured at 95°C for 5 min, and then separated by 10% sodium dodecyl sulfate-polyacrylamide gel electrophoresis (SDS-PAGE). Proteins were then transferred onto polyvinylidene difluoride (PVDF) membranes (Millipore) using a wet transfer system. Subsequently, the membranes were blocked with 5% skimmed milk in triple-phase buffered saline (TBST) containing 0.1% Tween-20 for 1 h at room temperature and then incubated overnight at 4°C with the following primary antibodies (all from Abcam, all at a dilution of 1 : 1000): P53, P21, cyclin E, CDK4, Rb, p-Rb, Bax, Bcl-2, caspase-3, SLC6A4, p-NF-κB, NF-κB, NLRP3, cleaved caspase-1 (C-caspase-1), GSDMD, IL-18, ASC, IL-1β, Nrf2, HO-1, and NQO1. GAPDH (1 : 5000) and lamin B (1 : 1000) were incubated overnight at 4°C as loading controls for cytoplasmic and nuclear protein, respectively. After washing the membrane, it was incubated with horseradish peroxidase (HRP)-conjugated secondary antibody (1 : 5000, Abcam) for 1 h at room temperature. Protein bands were visualized using an enhanced chemiluminescence (ECL) detection system (Thermo Fisher Scientific, USA) and imaged using a ChemiDoc MP imaging system (Bio-Rad, USA). Band intensity was quantified using ImageJ software. All experiments were independently repeated at least three times to ensure reproducibility. Data are expressed as normalized fold change to GAPDH (loading control) and presented as the mean ± SD of three independent runs.

Cell Counting Kit-8 (CCK-8) assay

To assess cell viability, CCK-8 (Dojindo Laboratories, Japan) was used according to the manufacturer's instructions [24]. H9c2 cells were seeded at a density of 5 × 10^3 per well into 100 µl of complete medium in 96-well plates and allowed to attach overnight under standard culture conditions (37°C, 5% CO_2). After treatment, 10 µl of CCK-8 reagent was added directly to each well and incubated at 37°C for 3 h. At the end of incubation, absorbance at 450 nm was measured using a microplate reader (Thermo Fisher Scientific, USA). Each condition was tested in at least three wells, and the whole experiment was repeated three times independently. Optical density (OD) values were used to calculate cell viability relative to the control, and the results were expressed as mean ± standard deviation.

Cell H/R model and treatment

To establish an H/R model *in vitro*, H9c2 cardiomyoblasts were first cultured in a hypoxia buffer solution and then placed in a triple-gas incubator with 1% O_2, 5% CO_2, and 94% N_2 for 2 h to effectively deplete residual oxygen from the environment. Subsequently, the cells were maintained in an anoxic state for 3 h at 37°C in a humidified atmosphere. At the end of the anoxic phase, the anoxic buffer was replaced with normoxic medium (DMEM with 10% FBS and 1% penicillin-streptomycin) and then reoxygenated for 2 h under standard culture conditions (21% O_2, 5% CO_2, 37°C). Experimental protocols for the H/R model were adapted from the method previously described by Wang *et al.* [31] with slight modifications for application in H9c2 cells.

Reactive oxygen species (ROS), superoxide dismutase (SOD), glutathione (GSH), malondialdehyde (MDA), lactate dehydrogenase (LDH), and adenosine triphosphate (ATP) detection

The kits used for measuring levels of ROS, GSH, MDA, ATP content, as well as SOD and LDH activities, were purchased from Beyotime Institute

of Biotechnology (Shanghai, China). Evaluation of ROS, GSH, MDA, ATP levels, and SOD and LDH activities in cells and cell supernatants was performed according to the manufacturer's protocol [24]. H9c2 cells were seeded in a 12-well plate at a density of 5×10^4 cells per well and treated with various concentrations of ropivacaine. Following treatment, the cells were incubated with dihydroethidine (DHE) for 60 min in the dark, as instructed in the assay kit. Subsequently, the fluorescence intensity was observed using a fluorescence microscope (Olympus, Japan), and the average OD was quantified using ImageJ software.

Statistical analysis

The statistical analysis was conducted using the R programming language. All experiments were independently repeated three times as biological replicates (n = 3), with three technical replicates per batch. The results are presented as the mean ± standard deviation (SD). A one-way ANOVA was used to assess the significance of the differences, and Tukey's post hoc test was applied for further analysis. A p-value less than 0.05 was the threshold for statistical significance [24, 32, 33].

Results

Identification and characterization of overlapping genes associated with MI and ropivacaine

The R package identified 915 upregulated DEGs and 586 downregulated DEGs from tissue samples and standard samples of the GSE97320 dataset (Figure 1 A). Subsequently, the Sangerbox platform identified three overlapping genes (*PCSK2*, *POMC*, and *SLC6A4*) from the up-regulated DEGs, down-regulated DEGs, and ropivacaine-related genes in the GSE97320 dataset (Figure 1 B). All three genes exhibited significant upregulation in the MI samples (Figure 1 C). The expression level

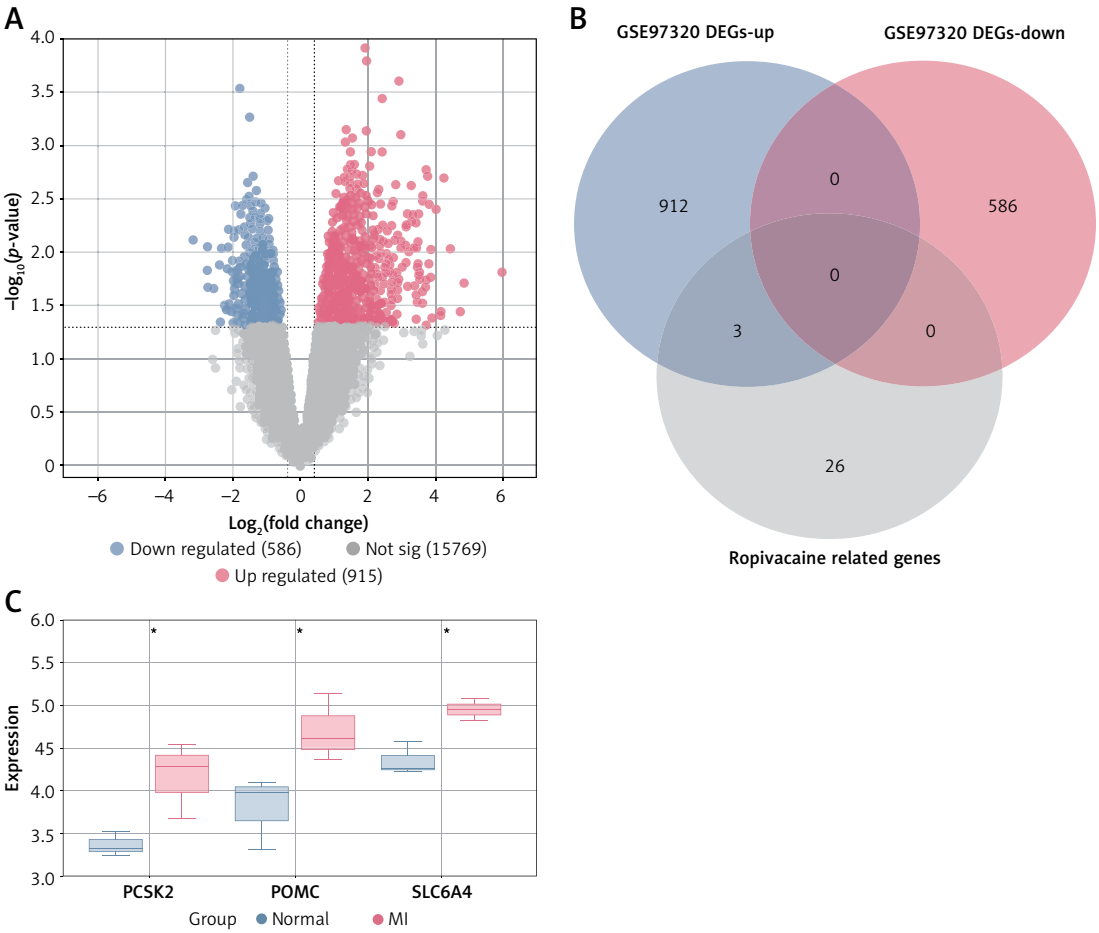

Figure 1. Identification and expression analysis of ropivacaine-related genes in the GSE97320 dataset. **A** – Volcano plot of differentially expressed genes (DEGs) in myocardial infarction (MI) versus control samples (n = 3 per group). Red: up-regulated DEGs; blue: down-regulated DEGs; gray: non-significant genes. Horizontal dashed line: $-\log_{10}(P) = 1.3$ ($p = 0.05$). **B** – Venn diagram showing the overlap between MI-up-regulated DEGs, MI-down-regulated DEGs, and ropivacaine-related genes. **C** – Heat map of the six overlapping DEGs in MI and control samples; row z-scores are color-coded (red = high, blue = low). Data are mean ± SD from three biological replicates per group. Statistical significance was assessed by one-way ANOVA followed by Tukey's multiple comparisons test (*$p < 0.05$)

of *PCSK2* was up-regulated from about 3.5 in the standard group to about 4.5 in the MI group, the expression level of *POMC* was up-regulated from about 4.0 in the standard group to about 4.5 in the MI group, and the expression level of *SLC6A4* was up-regulated from about 4.5 in the standard group to about 5.0 in the MI group. In addition, qPCR detection of the relative mRNA expression of *Pcsk2*, *Pomc*, and *Slc6a4* in the HR cell model showed that the expression levels of these genes were significantly upregulated under HR conditions. Specifically, the mRNA level of *Pcsk2* increased to approximately 1.3-fold of the control, the mRNA expression level of *Pomc* increased about 2-fold, and the mRNA expression level of *Slc6a4* increased about 3-fold (Supplementary Figure S1 A). These data further confirmed the significant upregulation of these genes under HR conditions. Given the critical role of *Slc6a4* in encoding serotonin transporter proteins, which are key to neurotransmission and have regulatory effects on the cardiovascular system, and its key role in MI and neurotoxicity has been extensively studied [34, 35], we chose to focus on *Slc6a4* to explore its potential protective role in ropivacaine-induced cellular injury.

Ropivacaine induces H9c2 cell cycle arrest in the G1 phase

Flow cytometry analysis revealed that treatment of H9c2 cells with ropivacaine at concentrations of 0.5 mM, 1 mM, and 2 mM for 24 h induced cell cycle arrest at the G1 phase (Figure 2 A). The percentage of G1 phase cells increased from approximately 50% to approximately 65% in the control group under 0.5 mM and 1 mM ropivacaine treatments, and significantly increased to approximately 70% under 2 mM treatment. We investigated key cell cycle regulators, including *Cdkn1a* (*p21*), *Ccne1* (*cyclin E*), and *Cdk4*, to further explore the potential regulatory mechanisms. qRT-PCR analysis demonstrated that with increasing concentrations of ropivacaine, the expression levels of *Cdkn1a* (p21) were significantly upregulated. The relative mRNA expression of *Cdkn1a* increased about 0.5-fold under 0.5 mM ropivacaine

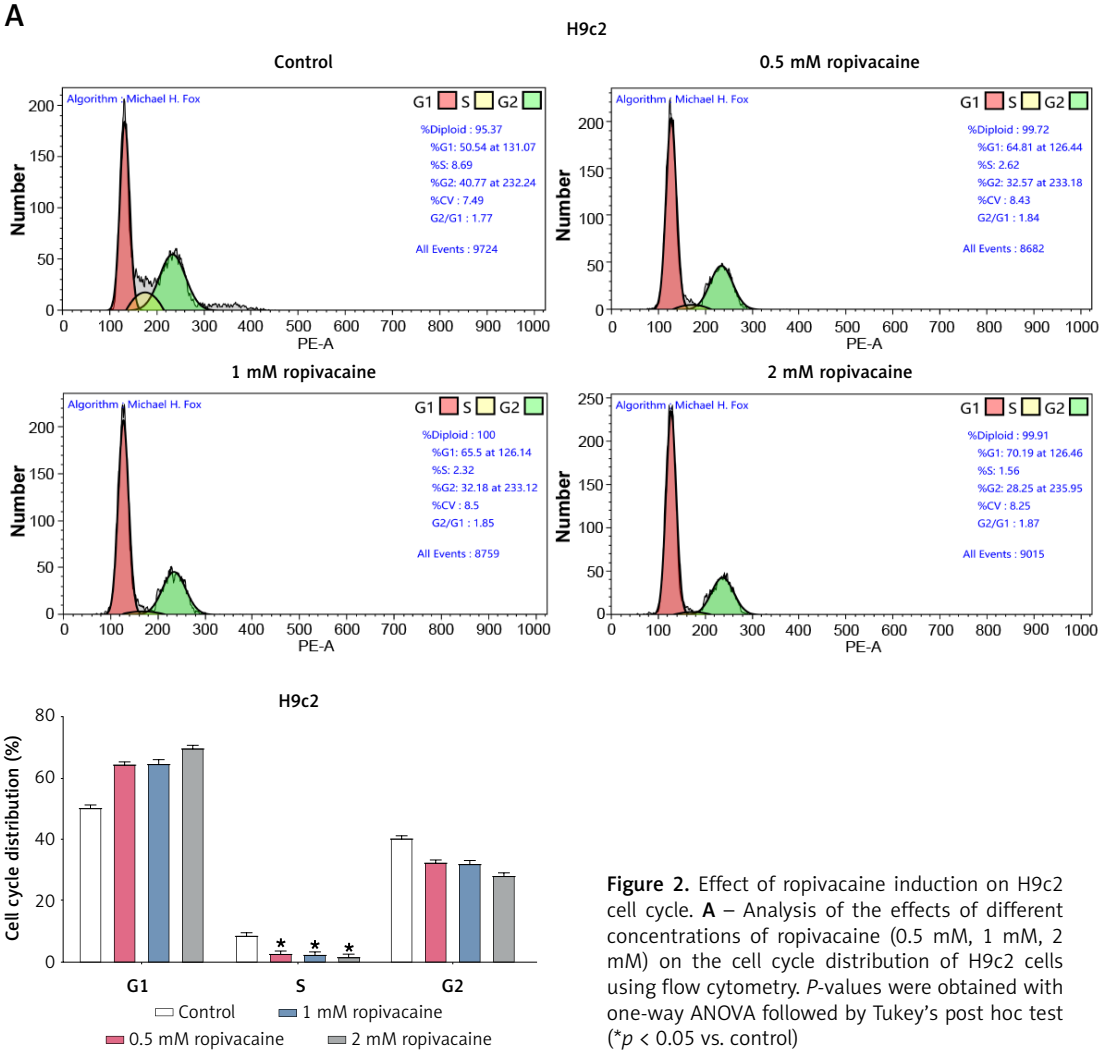

Figure 2. Effect of ropivacaine induction on H9c2 cell cycle. **A** – Analysis of the effects of different concentrations of ropivacaine (0.5 mM, 1 mM, 2 mM) on the cell cycle distribution of H9c2 cells using flow cytometry. *P*-values were obtained with one-way ANOVA followed by Tukey's post hoc test (*$p < 0.05$ vs. control)

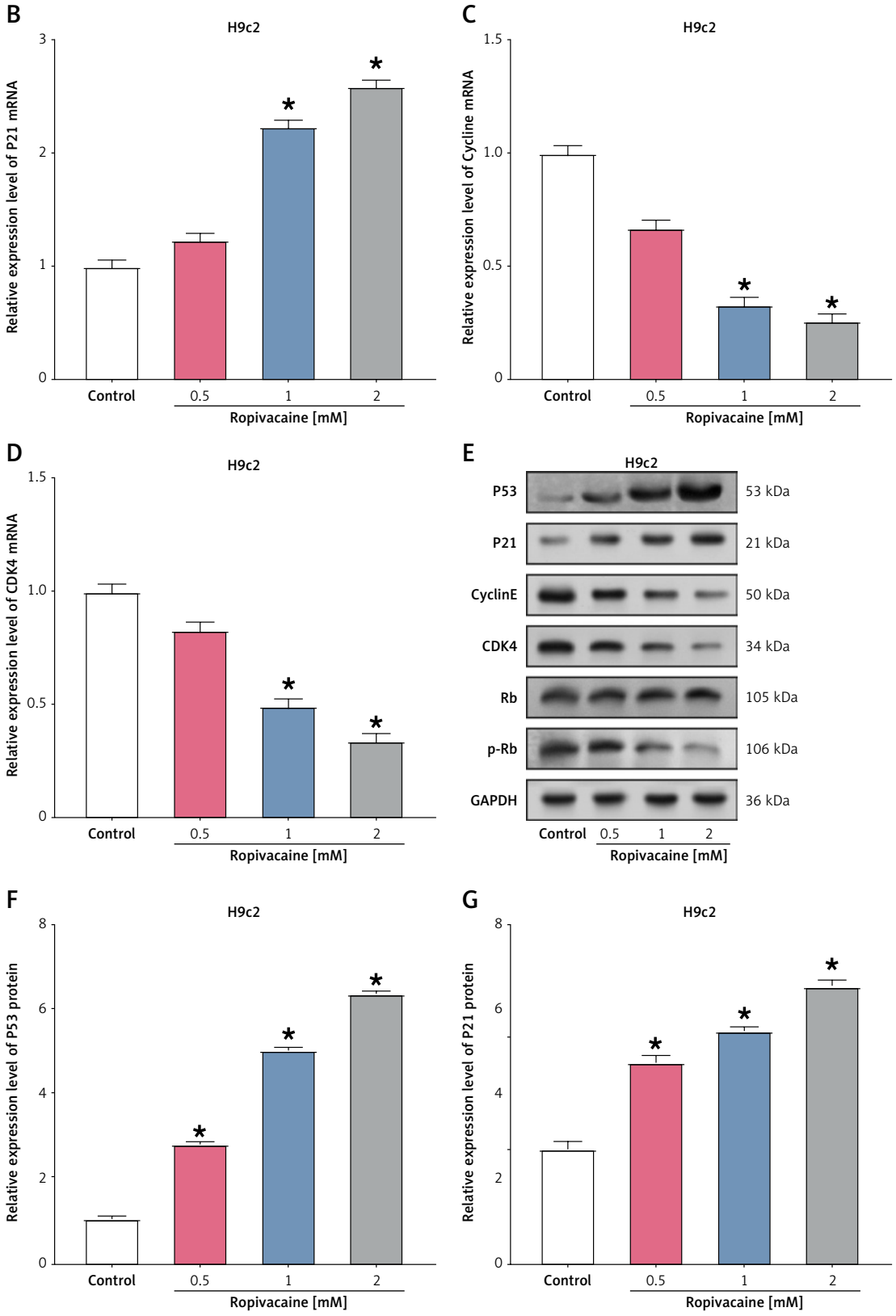

Figure 2. Cont. **B–D** – quantitative real-time polymerase chain reaction (qRT-PCR) analysis of the effects of different concentrations of Ropivacaine (0.5 mM, 1 mM, 2 mM) on the mRNA expression levels of *Cdkn1a (*p21*), Ccne1 (*cyclin E*),* and *Cdk4* in H9c2 cells, normalized to *Gapdh*. **E–G** – Western blot (WB) analyzed the effects of different concentrations of ropivacaine (0.5 mM, 1 mM, 2 mM) on the expression levels of P53, P21, cyclin E, CDK4, Rb, and p-Rb proteins in H9c2 cells, normalized to GAPDH. Data are mean ± SD from three independent experiments. *P*-values were obtained with one-way ANOVA followed by Tukey's post hoc test (*$p < 0.05$ vs. control)

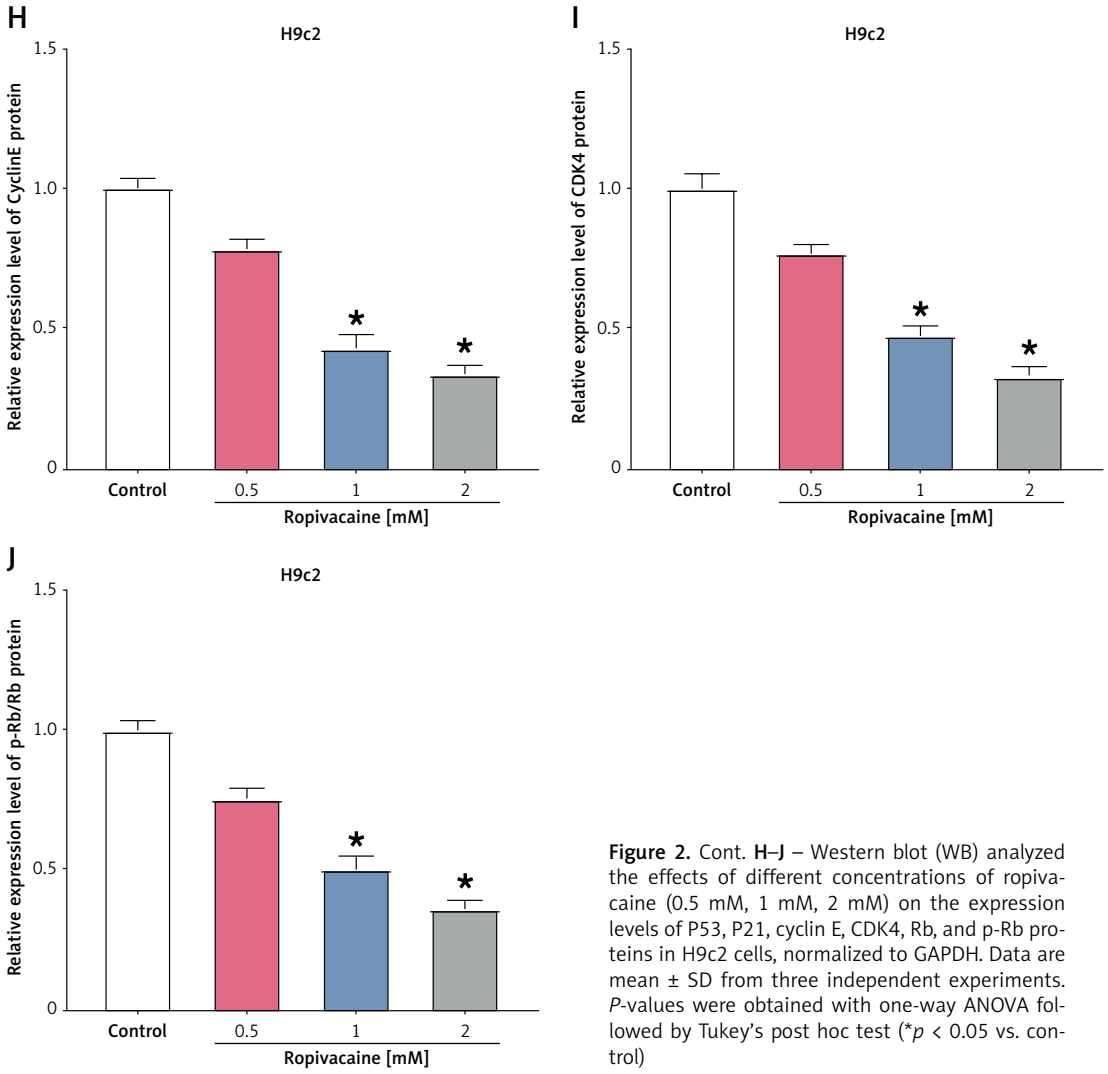

Figure 2. Cont. **H–J** – Western blot (WB) analyzed the effects of different concentrations of ropivacaine (0.5 mM, 1 mM, 2 mM) on the expression levels of P53, P21, cyclin E, CDK4, Rb, and p-Rb proteins in H9c2 cells, normalized to GAPDH. Data are mean ± SD from three independent experiments. *P*-values were obtained with one-way ANOVA followed by Tukey's post hoc test (*$p < 0.05$ vs. control)

treatment, about 1-fold under 1 mM ropivacaine treatment, and about 1.5-fold under 2 mM treatment (Figure 2 B). In contrast, the expression levels of *Ccne1* (*cyclin E*) and *Cdk4* were significantly downregulated. Under 0.5 mM ropivacaine treatment, the relative mRNA expression of *Ccne1* (*cyclin E*) was reduced by about 0.25-fold, and that of *Cdk4* was decreased by about 0.2-fold; under 1 mM ropivacaine treatment, the relative mRNA expression of *Ccne1* (*cyclin E*) was decreased by about 0.7-fold, and that of *Cdk4* was reduced by about 0.5-fold; under 2 mM treatment, the relative mRNA expression of *Ccne1* (*cyclin E*) was further reduced by about 0.8-fold and that of *Cdk4* by about 0.7-fold under 2 mM treatment (Figures 2 C, D). WB analysis showed that ropivacaine treatment significantly regulated the expression levels of key cell cycle regulatory proteins in H9c2 cells (Figures 2 E–J). Compared with the control group, treatment with 0.5 mM ropivacaine resulted in an approximately 1.5-fold increase in P53 protein expression and a 0.8-fold increase in P21 protein expression. At 1 mM ropivacaine, P53 expression increased by approximately 4-fold, while P21 expression increased by about 1-fold. Under 2 mM ropivacaine treatment, P53 expression increased by approximately 5-fold, and P21 expression increased by around 1.5-fold. These data suggest that ropivacaine may have promoted G1 phase arrest by upregulating the expression of P53 and P21. Meanwhile, the expression levels of cyclin E, CDK4, and p-Rb proteins were significantly decreased under ropivacaine treatment. Under 0.5 mM ropivacaine treatment, the relative expression of cyclin E and p-Rb proteins was reduced by about 0.2-fold, and the relative expression of CDK4 protein was decreased by about 0.3-fold; under 1 mM ropivacaine treatment, the relative expression of cyclin E, p-Rb and CDK4 proteins was reduced by about 0.5-fold; under 2 mM treatment, the relative expression of cyclin E, p-Rb and CDK4 proteins decreased about 0.6-fold. These results suggest that ropivacaine further promotes G1 phase arrest by down-regulating the expres-

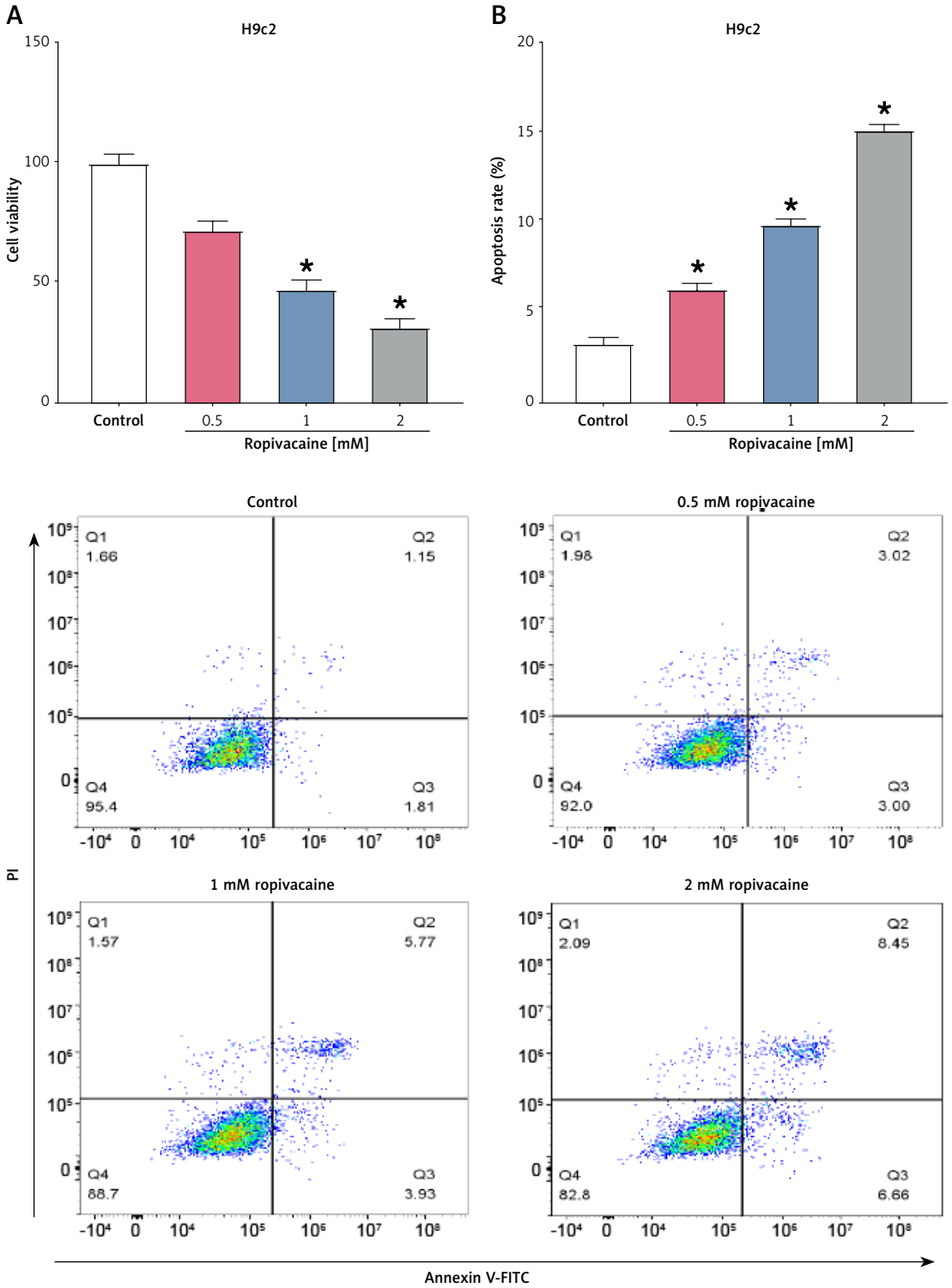

Figure 3. Apoptosis of H9c2 cells induced by ropivacaine. **A** – Cell Counting Kit-8 (CCK-8) analysis evaluating the effects of different concentrations of ropivacaine (0.5 mM, 1 mM, 2 mM) on the viability of H9c2 cells. **B** – Analysis of the effects of different concentrations of ropivacaine (0.5 mM, 1 mM, 2 mM) on the apoptosis of H9c2 cells through flow cytometry. *P*-values were obtained with one-way ANOVA followed by Tukey's post hoc test (*$p < 0.05$ vs. control)

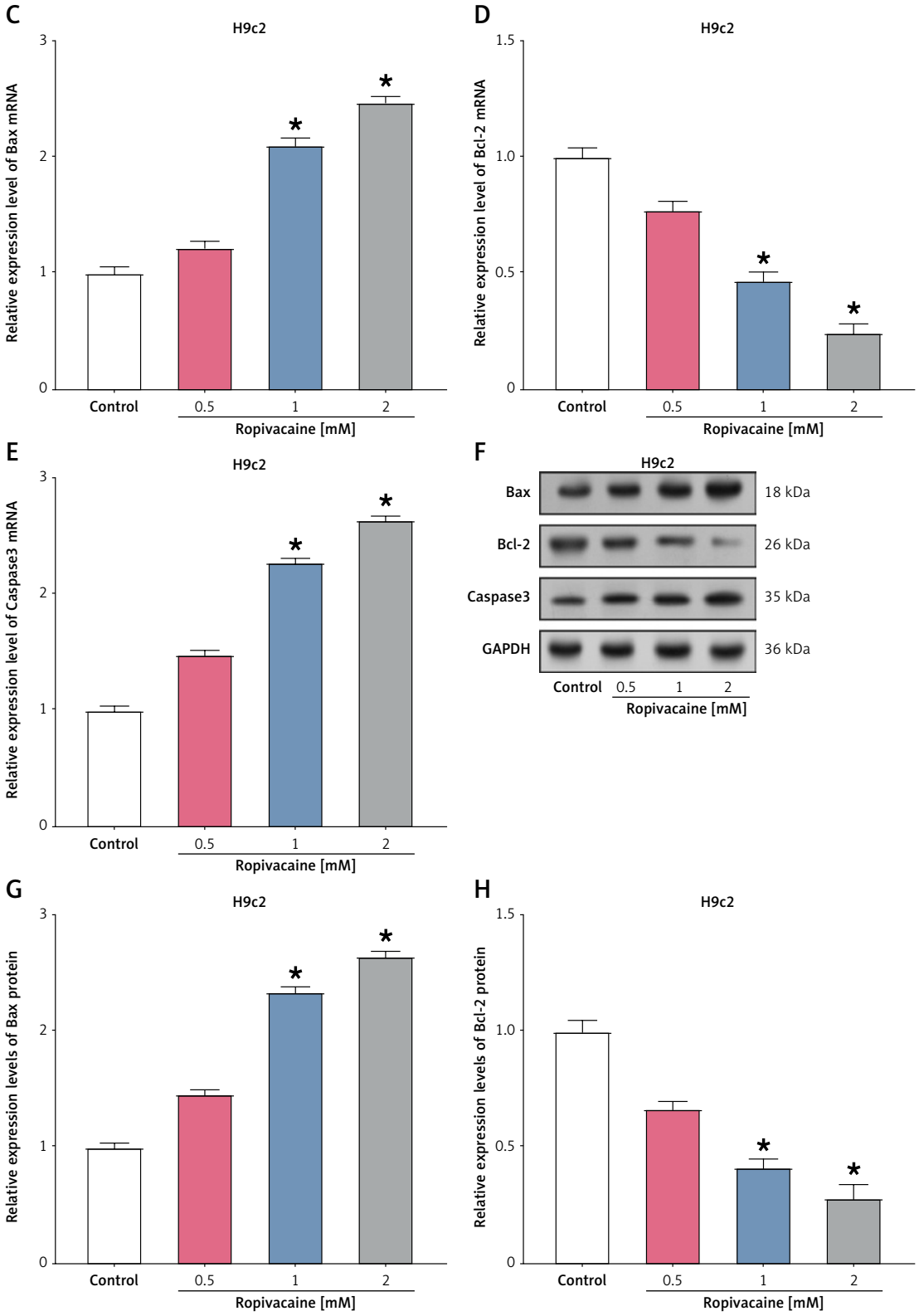

Figure 3. Cont. **C–E** – qRT-PCR analysis of the effects of different concentrations of ropivacaine (0.5 mM, 1 mM, 2 mM) on the mRNA expression levels of *Bax*, *Bcl2*, and *Casp3* in H9c2 cells, normalized to *Gapdh*. **F–H** – WB analysis of the effects of different concentrations of ropivacaine (0.5 mM, 1 mM, 2 mM) on protein expression levels of Bax, Bcl-2, and caspase-3 in H9c2 cells, normalized to GAPDH. Data are mean ± SD from three independent experiments. *P*-values were obtained with one-way ANOVA followed by Tukey's post hoc test (*$p < 0.05$ vs. control)

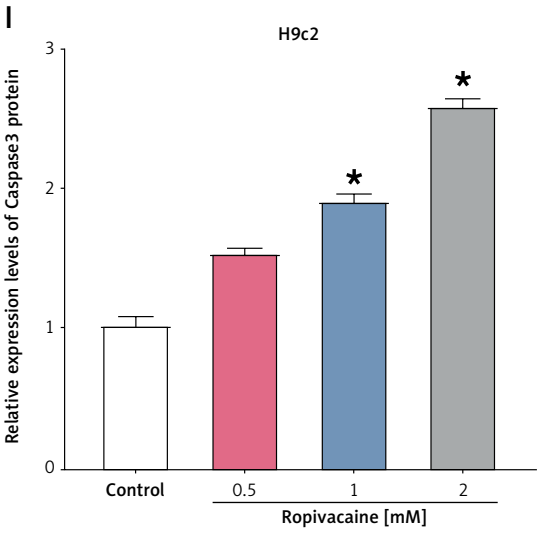

Figure 3. Cont. **I** – WB analysis of the effects of different concentrations of ropivacaine (0.5 mM, 1 mM, 2 mM) on protein expression levels of Bax, Bcl-2, and caspase-3 in H9c2 cells, normalized to GAPDH. Data are mean ± SD from three independent experiments. *P*-values were obtained with one-way ANOVA followed by Tukey's post hoc test (*$p < 0.05$ vs. control)

sion of cell cycle protein E, CDK4, and p-Rb. In addition, ropivacaine may act by interfering with the p53 and Rb signaling pathways.

Ropivacaine induces apoptosis of H9c2 cells

The CCK-8 assay showed a significant decrease in H9c2 cell viability with increasing concentrations of ropivacaine. At a concentration of 0.5 mM, cell viability decreased to approximately 75%, further reduced to approximately 50% at 1 mM, and decreased to approximately 30% at a concentration of 2 mM (Figure 3 A). Correspondingly, flow cytometry analysis demonstrated a significant increase in cell apoptosis with escalating concentrations of ropivacaine. The apoptosis rate increased by approximately 3% at 0.5 mM, 6% at 1 mM, and 12% at 2 mM (Figure 3 B). The proteins Bax and caspase-3, known to promote apoptosis, and Bcl-2, which has an anti-apoptotic effect, were quantified. Both qRT-PCR and WB analysis showed that with increasing concentrations of ropivacaine, *Bax* expression levels increased approximately 0.1-fold at 0.5 mM, approximately 1-fold at 1 mM, and approximately 1.5-fold at 2 mM (Figures 3 C, G). Caspase-3 expression levels increased approximately 0.5-fold at 0.5 mM, 1-fold at 1 mM, and 1.5-fold at 2 mM (Figures 3 E, I). In contrast, Bcl-2 expression levels decreased approximately 0.2-fold at 0.5 mM concentration, 0.5-fold at 1 mM concentration, and approximately 0.8-fold at 2 mM concentration (Figures 3 D, H). These data suggest that ropivacaine induces apoptosis in H9c2 cells by up-regulating the expression of *Bax* and caspase-3 and down-regulating the expression of Bcl-2.

Ropivacaine induces oxidative stress in H9c2 cells

To gain a deeper understanding of the effects of ropivacaine on the level of oxidative stress in H9c2 cells, we systematically measured several key biochemical indices, including the activities of SOD and LDH, the content of MDA, GSH, and ATP, as well as the level of intracellular ROS. Compared to untreated controls, ropivacaine significantly increased intracellular ROS levels dose-dependently. Ropivacaine significantly increased intracellular ROS levels by approximately 0.25-fold at a 0.5 mM concentration, by approximately 1-fold at a 1 mM concentration, and by approximately 1.5-fold at a 2 mM concentration (Figure 4 A). MDA levels increased by approximately 0.1-fold at the 0.5 mM concentration and by approximately 1.5-fold at the 1 mM concentration. MDA levels increased approximately 0.1-fold at 0.5 mM, 1.2-fold at 1 mM, and 2-fold at 2 mM (Figure 4 D). LDH activity increased approximately 0.5-fold at 0.5 mM, 1-fold at 1 mM, and 2-fold at 2 mM (Figure 4 E). In contrast, a decrease in SOD activity was observed, with SOD activity decreasing ~0.1-fold at 0.5 mM, ~0.5-fold at 1 mM, and ~0.75-fold at 2 mM (Figure 4 B). GSH levels decreased ~0.15-fold at 0.5 mM, ~0.5-fold at 1 mM, and ~0.75-fold at 2 mM (Figure 4 C). ATP levels decreased approximately 0.16-fold at 0.5 mM, 0.6-fold at 1 mM, and 0.7-fold at 2 mM (Figure 4 F). In conclusion, these results indicate that ropivacaine promotes oxidative stress in H9c2 cells, not only revealing the significant effect of ropivacaine on the redox homeostasis of H9c2 cells but also highlighting its potential impact on the cellular energy metabolic state.

Knocking down *Slc6a4* has an anti-apoptotic effect and protects H9c2 cells from ropivacaine and H/R-induced damage

qRT-PCR and WB analyses showed that the expression level of *Slc6a4* in H9c2 cells increased significantly with increasing concentrations of ropivacaine. si-*Slc6a4* expression levels increased approximately 0.2-fold at 0.5 mM, 1.1-fold at 1 mM, and 1.9-fold at 2 mM (Figures 5 A, B). Subsequent knockdown experiments using si-*Slc6a4*-1 showed that it was more efficient. Therefore, it was selected for subsequent experiments. si-*Slc6a4*-1 showed a knockdown efficiency of about 90%, while si-*Slc6a4*-2 showed a knockdown efficiency of about 70% (Figures 5 C, D). The CCK-8 assay showed that the combined treatment of HR and 2 mM ropivacaine significantly reduced the

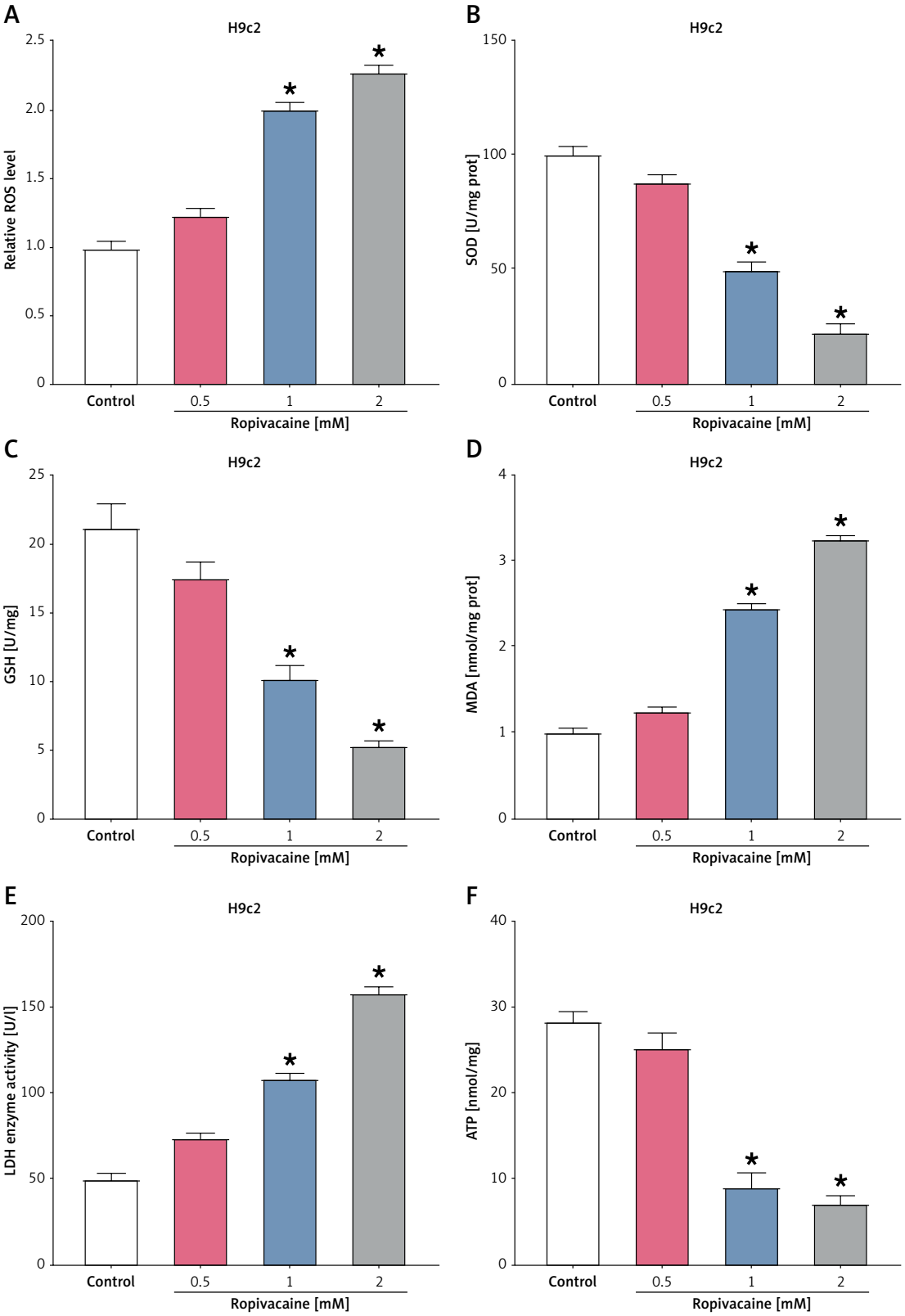

Figure 4. Oxidative stress of H9c2 cells induced by ropivacaine. **A**–**F** – Commercial diagnostic reagent kit analyzing the effects of different concentrations of ropivacaine (0.5 mM, 1 mM, 2 mM) on levels of reactive oxygen species (ROS), superoxide dismutase (SOD), glutathione (GSH), malondialdehyde (MDA), lactate dehydrogenase (LDH), and adenosine triphosphate (ATP) in H9c2 cells. Data are mean ± SD from three independent experiments. *P*-values were obtained with one-way ANOVA followed by Tukey's post hoc test (*$p < 0.05$ vs. control)

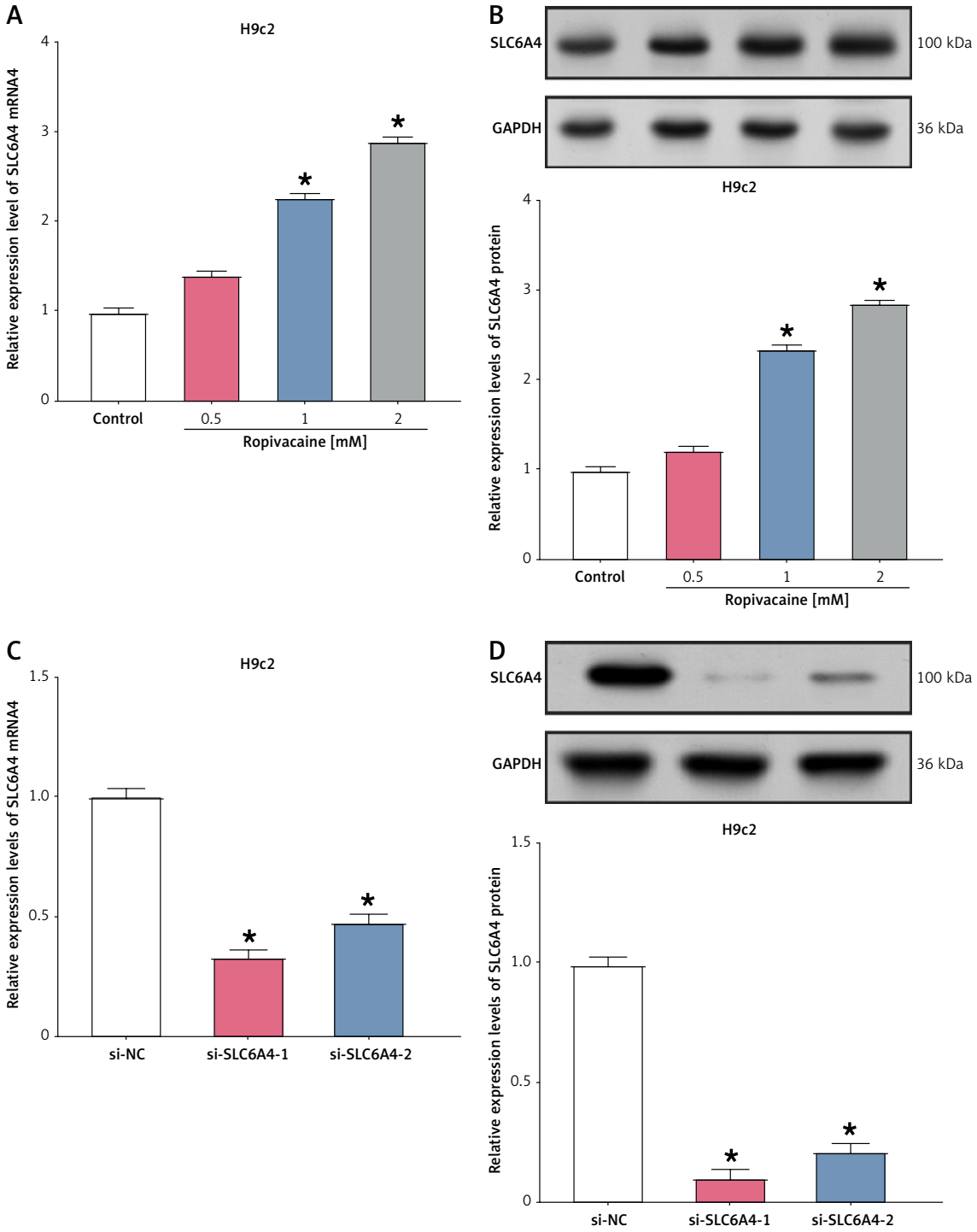

Figure 5. Effects of *Slc6a4* knockdown on cell viability and apoptosis after ropivacaine treatment under hypoxia/reoxygenation (H/R) conditions. **A** – Effect of different concentrations of ropivacaine (0.5 mM, 1 mM, 2 mM) on the expression levels of *Slc6a4* mRNA in H9c2 cells was analyzed by qRT-PCR, normalized to *Gapdh*. **B** – WB analysis of the effects of different concentrations of ropivacaine (0.5 mM, 1 mM, 2 mM) on expression levels of SLC6A4 protein in H9c2 cells, normalized to GAPDH. **C** – qRT-PCR analysis of *Slc6a4* knockdown in H9c2 cells treated with different concentrations of ropivacaine (0.5 mM, 1 mM, 2 mM), normalized to *Gapdh*. **D** – WB analysis of *Slc6a4* knockdown in H9c2 cells treated with different concentrations of ropivacaine (0.5 mM, 1 mM, 2 mM), normalized to GAPDH. *P*-values were obtained with one-way ANOVA followed by Tukey's post hoc test (*$p < 0.05$ vs. control, $^{\#}p < 0.05$ vs. HR + 2 mM ropivacaine + small interfering RNA negative control (si-NC))

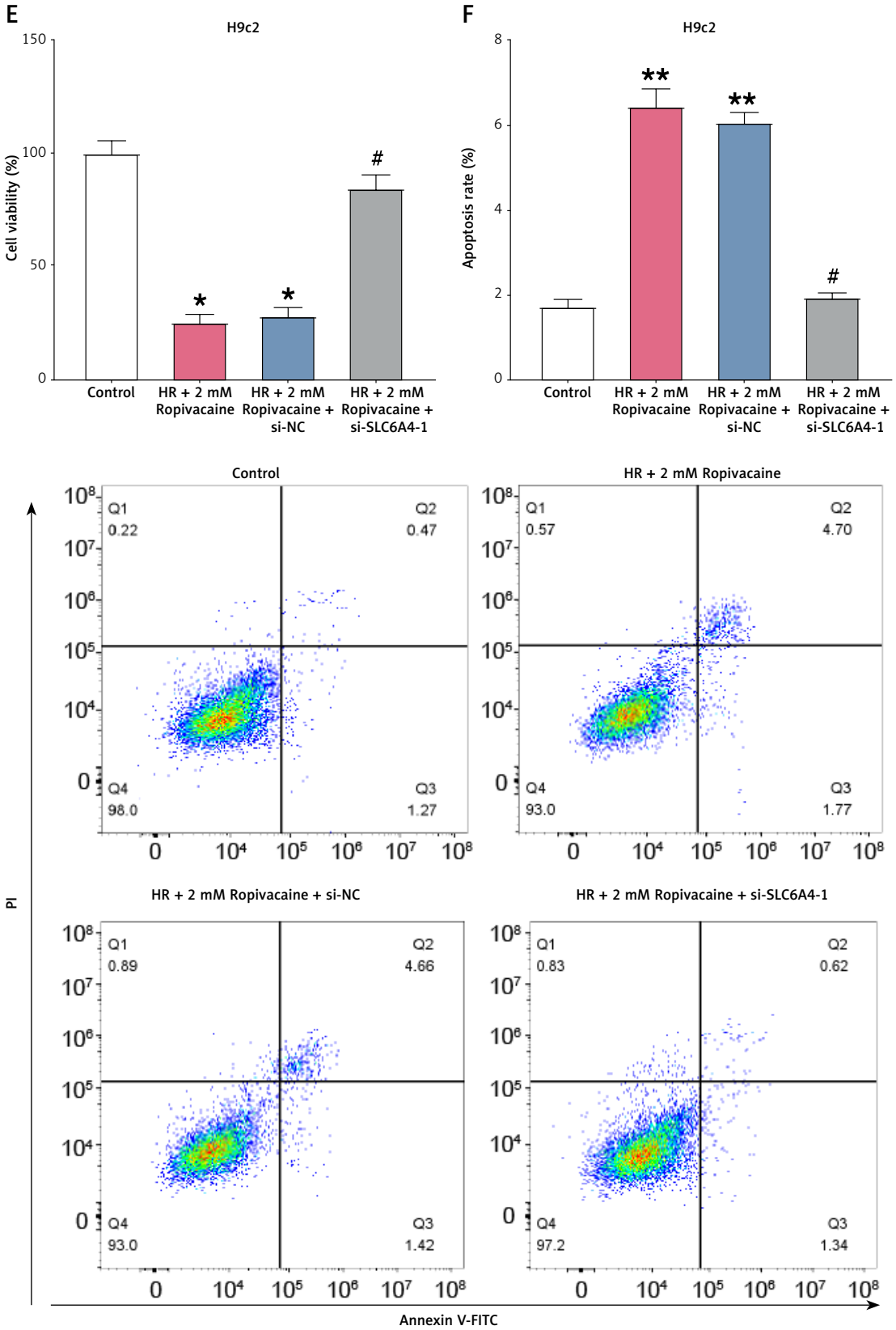

Figure 5. Cont. **E** – Analysis of CCK-8 examining the effects of *Slc6a4* knockdown on the viability of H9c2 cells induced by H/R combined with 2 mM ropivacaine. **F** – Analysis of flow cytometry on the effects of *Slc6a4* knockdown versus non-knockdown on H/R combined with 2 mM ropivacaine-induced apoptosis in H9c2 cells. Data are mean ± SD from three independent experiments. *P*-values were obtained with one-way ANOVA followed by Tukey's post hoc test (*$p < 0.05$ vs. control, #$p < 0.05$ vs. HR + 2 mM ropivacaine + small interfering RNA negative control (si-NC))

viability of H9c2 cells, which was attenuated by the addition of si-*Slc6a4*-1. H/R and 2 mM ropivacaine co-treatment decreased cell viability to approximately 25%, while adding si-*Slc6a4*-1 restored cell viability to approximately 80% (Figure 5 E). Similarly, flow cytometry analysis revealed that the combined treatment of HR and 2 mM ropivacaine significantly increased apoptosis in H9c2 cells, which was alleviated by the addition of si-*Slc6a4*-1. The apoptosis rate increased by approximately 5% after the combined treatment of HR and 2 mM ropivacaine, while it decreased by approximately 4% after the addition of si-*Slc6a4*-1 (Figure 5 F). These results suggest that *Slc6a4* plays a crucial role in ropivacaine-induced damage to H9c2 cells, and the knockdown of *Slc6a4* partially attenuates this damage.

Slc6a4 knockdown attenuates the ropivacaine-induced inflammatory response in H9c2 cells by inhibiting NLRP3 inflammatory vesicle activation

NF-κB, p-NF-κB, NLRP3, cleaved caspase-1 (C-caspase-1), GSDMD, IL-18, ASC, and IL-1β are proteins associated with the NLRP3 inflammasome. Western blot analysis showed that under HR + 2 mM ropivacaine treatment, the expression levels of p-NF-κB were significantly upregulated by ~4.8-fold, NLRP3 by ~5-fold, C-caspase-1 by ~3.8-fold, GSDMD by ~2.8-fold, IL-18 by ~2.5-fold, ASC by ~3.5-fold, and IL-1β by ~2-fold. However, treatment with si-*Slc6a4*-1 or the NLRP3 inhibitor MCC950 markedly downregulated the expression levels of p-NF-κB, NLRP3, GSDMD, IL-1β, and ASC by ~0.6-fold, and C-caspase-1 and IL-18 by ~0.5-fold. The above results show that the expression level of NLRP3, an inflammatory vesicle-associated protein, was significantly upregulated in H9c2 cells after co-treatment with H/R conditions and 2 mM ropivacaine. However, this upregulation effect was significantly attenuated when specific si-*Slc6a4*-1 was added to reduce *Slc6a4* expression. Moreover, the results obtained by using the NLRP3 inflammatory vesicle inhibitor MCC950 were similar to the effect of knocking down *Slc6a4*, suggesting that the knockdown of *Slc6a4* may effectively inhibit the increase in NLRP3 inflammatory vesicle-associated protein expression induced by ropivacaine (Figures 6 A–G). In addition, the qPCR detection of mRNA expression levels for two inflammatory factors, *Il18* and *Il1b*,

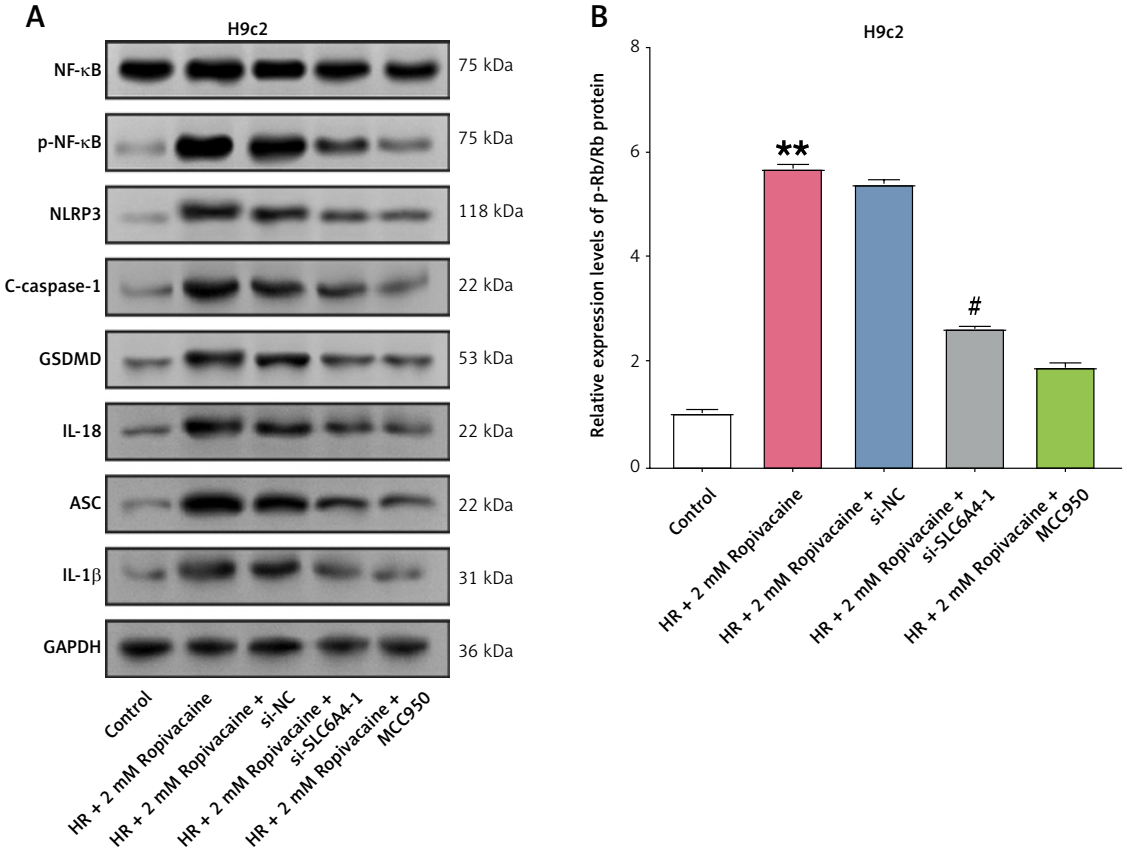

Figure 6. Effects of *Slc6a4* knockdown in H9c2 cells under H/R conditions on ropivacaine-induced NLRP3 inflammasome activation. **A–B** – WB analysis of *Slc6a4* knockdown or addition of MCC950 on protein expression levels of NF-κB, p-NF-κB, NLRP3, C-caspase-1, GSDMD, IL-18, ASC, and IL-1β in H9c2 cells induced by 2 mM ropivacaine under hypoxia/reoxygenation conditions, normalized to GAPDH. Data are mean ± SD from three independent experiments. *P*-values were obtained with one-way ANOVA followed by Tukey's post hoc test (**p* < 0.05 vs. Control, #*p*< 0.05 vs. HR + 2 mM Ropivacaine + si-NC)

si-SLC6A4-1 – small interfering RNA targeting SLC6A4; MCC950 – NLRP3 inflammasome inhibitor.

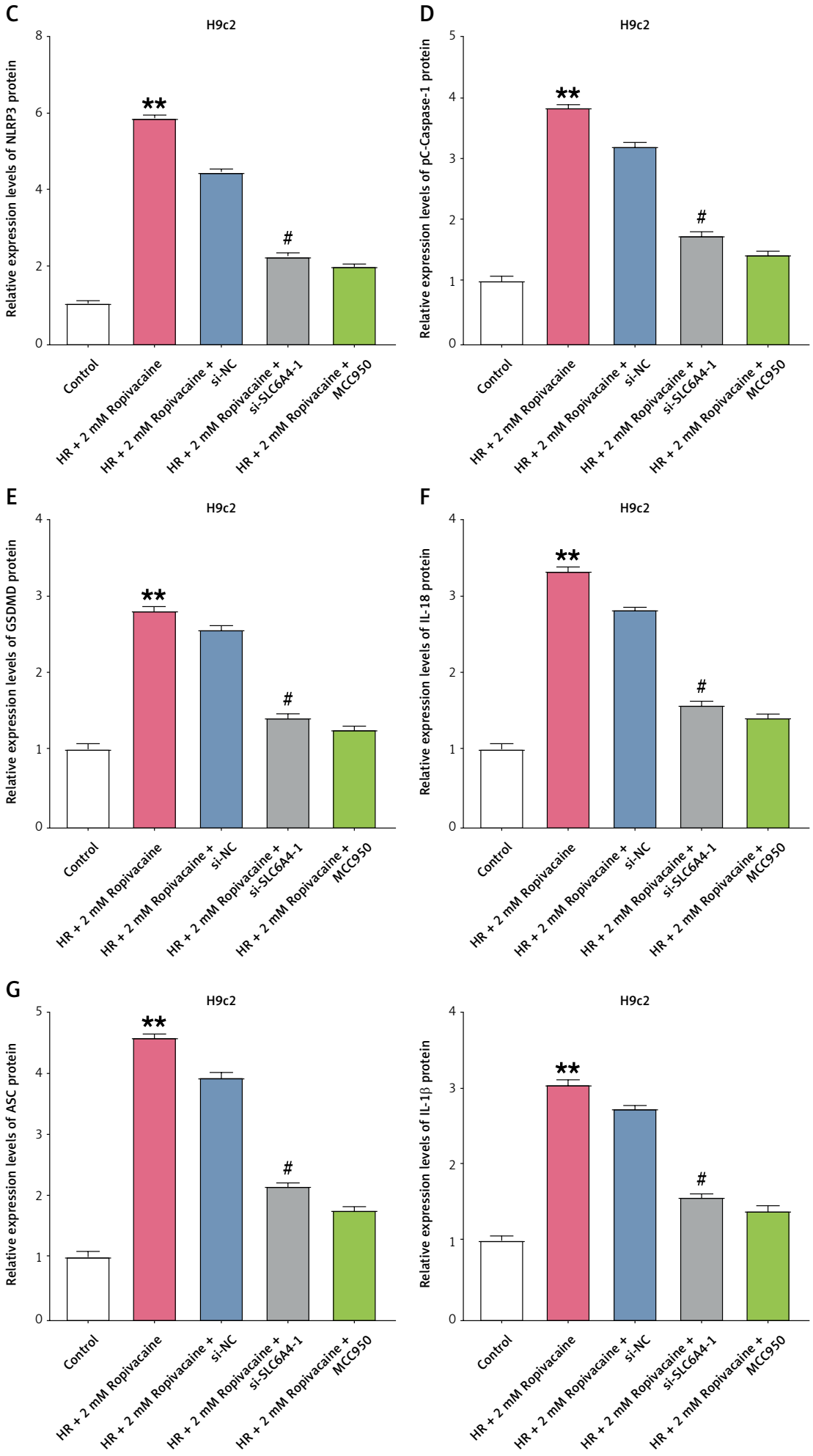

Figure 6. Cont. **C–G** – WB analysis of *Slc6a4* knockdown or addition of MCC950 on protein expression levels of NF-κB, p-NF-κB, NLRP3, C-caspase-1, GSDMD, IL-18, ASC, and IL-1β in H9c2 cells induced by 2 mM ropivacaine under hypoxia/reoxygenation conditions, normalized to GAPDH. Data are mean ± SD from three independent experiments. *P*-values were obtained with one-way ANOVA followed by Tukey's post hoc test (*$p < 0.05$ vs. Control, #$p < 0.05$ vs. HR + 2 mM Ropivacaine + si-NC)

si-SLC6A4-1 – small interfering RNA targeting SLC6A4; MCC950 – NLRP3 inflammasome inhibitor.

yielded results similar to those obtained from WB detection, further validating our findings (Supplementary Figures S1 B, C). Under HR + 2 mM ropivacaine treatment, the mRNA expression level of *Il18* was significantly increased by about 2.9-fold, while that of *Il1b* was significantly increased by about 3-fold. However, after adding si-*Slc6a4*-1 or the NLRP3 inhibitor MCC950, the mRNA expression level of *Il18* was significantly decreased by about 2.9-fold, whereas the mRNA expression level of *IL-1*β decreased by about 3-fold.

Protective role of *Slc6a4* in ropivacaine-induced H9c2 cell injury by promoting Nrf2 nuclear translocation and its downstream antioxidant gene expression

To investigate whether the *Slc6a4*-induced anti-apoptotic effect is associated with Nrf2 nuclear translocation, we performed WB analysis to determine cytoplasmic and nuclear Nrf2 protein levels. The data showed that co-treatment with HR and 2 mM ropivacaine decreased cytoplasmic Nrf2 levels and increased nuclear Nrf2 levels compared to the control group. Cytoplasmic Nrf2 levels decreased to approximately 1-fold with HR and 2 mM ropivacaine treatment, while nuclear Nrf2 levels increased to approximately 2.5-fold (Figures 7 A–C). However, adding si-*Slc6a4*-1 further decreased the cytoplasmic Nrf2 level by about 1.8-fold, while the nuclear Nrf2 level increased by about 5.5-fold (Figures 7 A–C). Additionally, we examined the protein expression levels of Nrf2's downstream target genes, HO-1 and NQO1. The results showed that the expression levels of HO-1 and NQO1 were significantly up-regulated by the combined treatment of HR and 2 mM ropivacaine. The expression levels of HO-1 were increased to approximately 1.5-fold, and those of NQO1 were increased to approximately 1-fold by treating HR with 2 mM ropivacaine (Figures 7 D–F). Upon the addition of si-*Slc6a4*-1, the expression levels of HO-1 and NQO1 were further increased to approximately 2.8-fold for HO-1 and 3.6-fold for NQO1 (Figures 7 D–F). To further validate the protective role of *Slc6a4* in ropivacaine-induced H9c2 cell injury via the Nrf2 signaling pathway, we performed experiments using the Nrf2 inhibitor ML385. Flow cytometry analysis revealed that combining HR and 2 mM ropivacaine treatment significantly increased the rate of apoptosis. The apoptosis rate in the HR and 2 mM ropivacaine-treated group increased to approximately 9% compared to the control group. The addition of si-*Slc6a4*-1 significantly reduced the apoptosis rate to approximately 2%. However, when ML385 inhibited Nrf2, the anti-apoptotic effect of si-*Slc6a4*-1 was attenuated considerably, and the apoptotic rate increased again to approximately 4% (Figures 7 G, H). These results suggest that the silencing of *Slc6a4* may be related to the enhanced nuclear translocation of Nrf2 and the increased expression of its down-

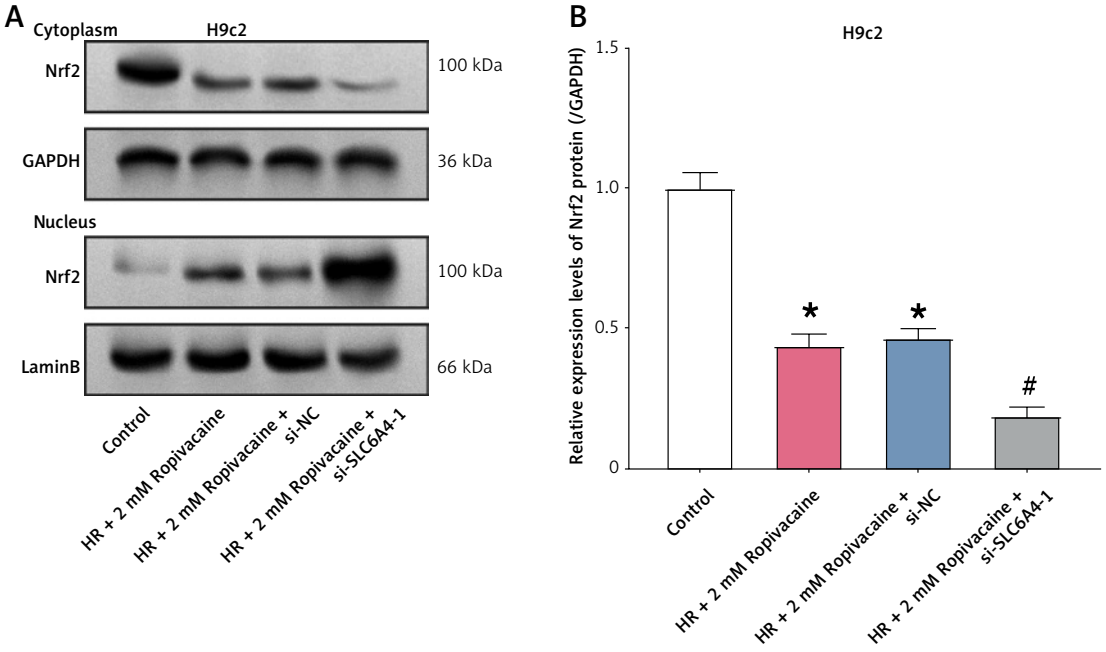

Figure 7. Effect of *Slc6a4* knockdown on ropivacaine-induced Nrf2 nuclear translocation and apoptosis in H9c2 cells under H/R conditions. **A**–**B** – WB analysis of *Slc6a4* knockdown's effect on protein expression levels of Nrf2 in the cytoplasm and nucleus of H9c2 cells induced by 2 mM ropivacaine under H/R conditions. GAPDH and lamin B were used as internal controls for the cytoplasm and the nucleus, respectively. *p* values were obtained with one-way ANOVA followed by Tukey's post hoc test (*$p < 0.05$ vs. control, #$p < 0.05$ vs. HR + 2 mM ropivacaine + si-NC, &$p < 0.05$ vs. HR + 2 mM ropivacaine + si-*Slc6a4* + ML385)

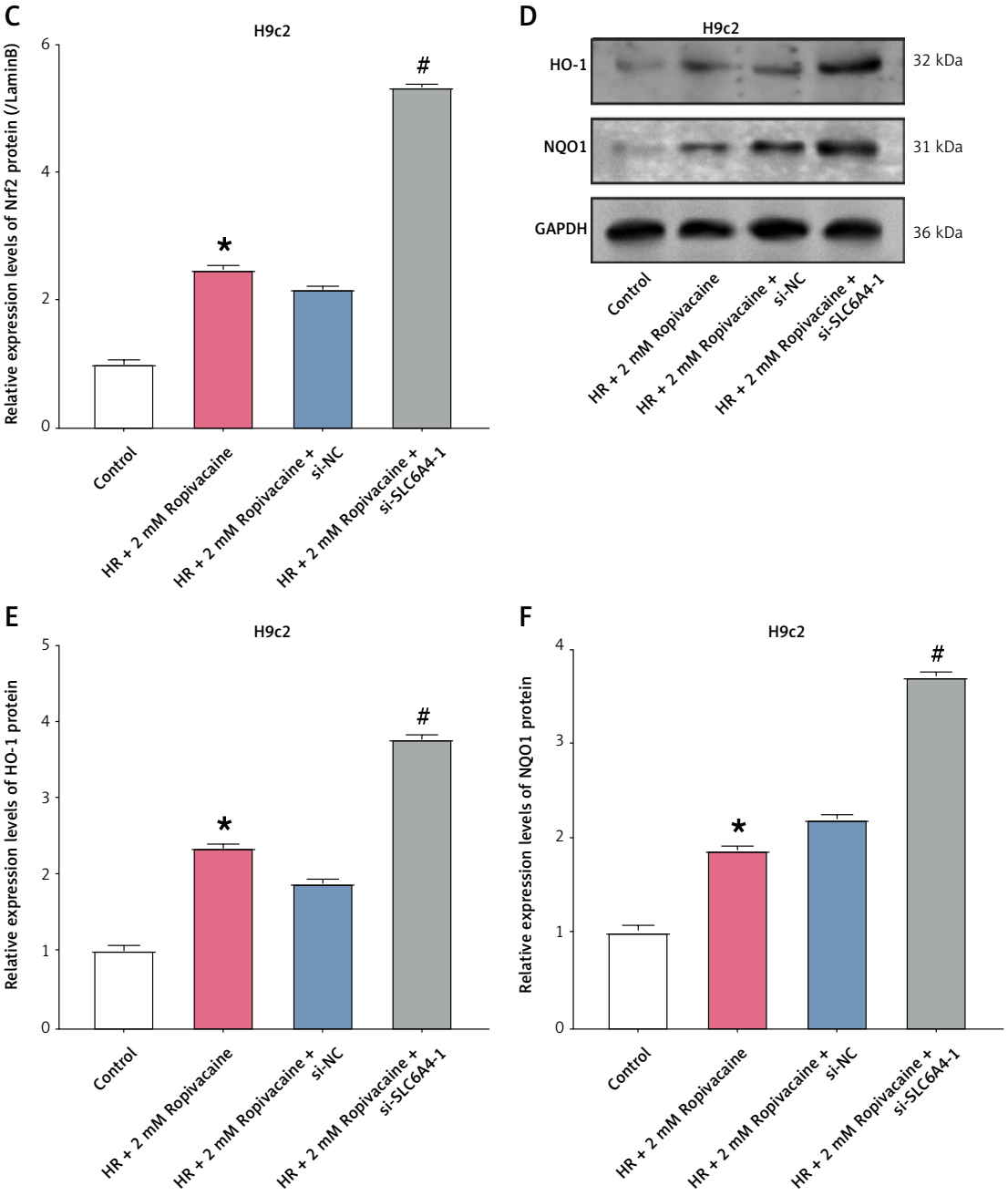

Figure 7. Cont. **C** – WB analysis of *Slc6a4* knockdown's effect on protein expression levels of Nrf2 in the cytoplasm and nucleus of H9c2 cells induced by 2 mM ropivacaine under H/R conditions. GAPDH and lamin B were used as internal controls for the cytoplasm and the nucleus, respectively. **D–F** – WB analysis on the effects of silencing *Slc6a4* on protein expression levels of HO-1 and NQO1 in H9c2 cells induced by 2 mM ropivacaine under hypoxia/reoxygenation conditions, normalized to GAPDH. *p* values were obtained with one-way ANOVA followed by Tukey's post hoc test (**p* < 0.05 vs. control, #*p*< 0.05 vs. HR + 2 mM ropivacaine + si-NC, &*p* < 0.05 vs. HR + 2 mM ropivacaine + si-*Slc6a4* + ML385)

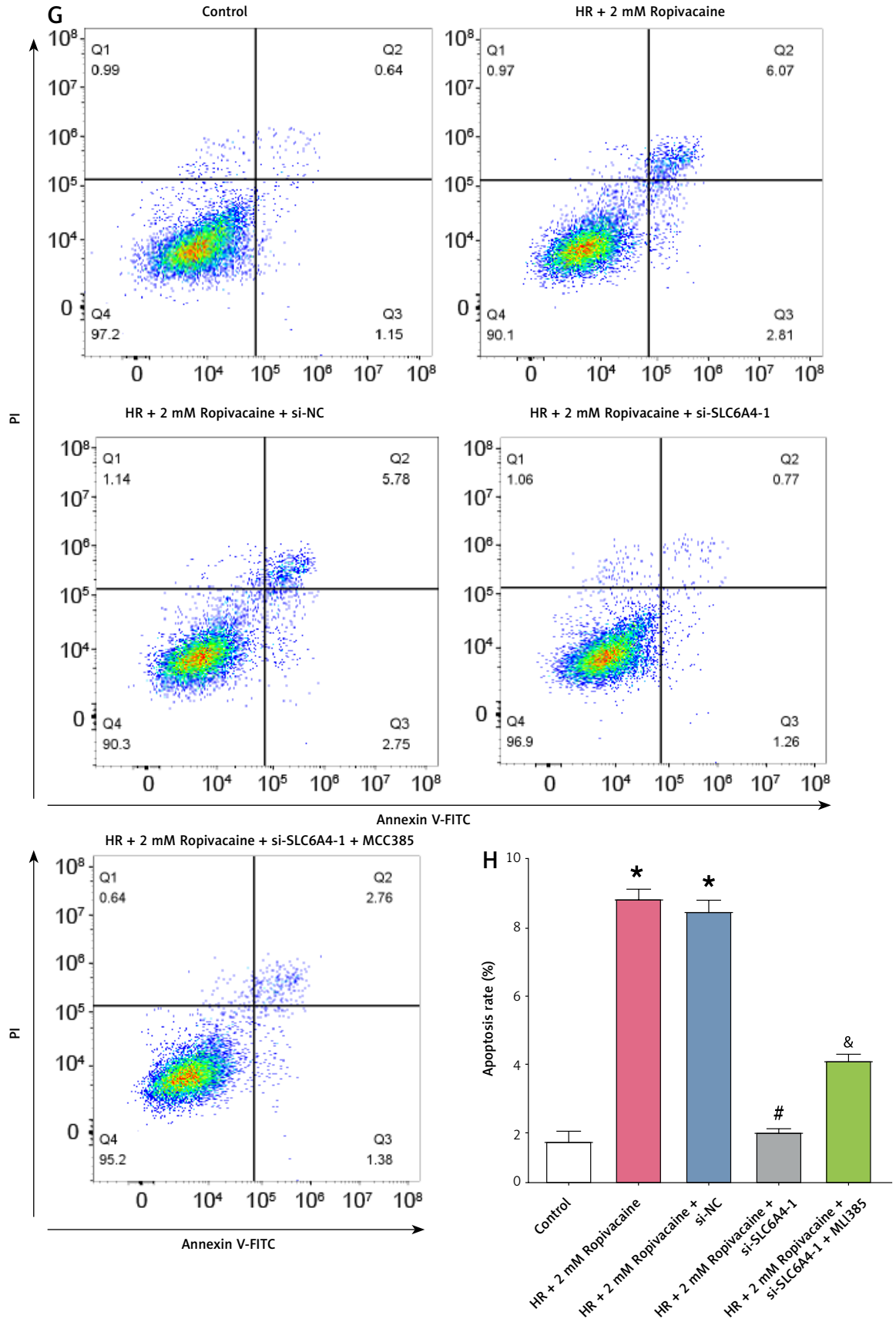

Figure 7. Cont. **G**, **H** – Flow cytometry analysis of the impact of *Slc6a4* knockdown or the addition of nuclear factor erythroid 2-related factor 2 inhibitor (ML385) on H/R combined with 2 mM ropivacaine-induced apoptosis in H9c2 cells. Data are mean ± SD from three independent experiments. *p* values were obtained with one-way ANOVA followed by Tukey's post hoc test (*$p < 0.05$ vs. control, #$p < 0.05$ vs. HR + 2 mM ropivacaine + si-NC, &$p < 0.05$ vs. HR + 2 mM ropivacaine + si-*Slc6a4* + ML385)

stream antioxidant genes, thereby playing a protective role in ropivacaine-induced H9c2 cell injury, a process that may involve the activation of the Nrf2 signaling pathway.

Discussion

MI occurs when blood flow to a portion of the heart is obstructed, leading to myocardial ischemia and tissue necrosis [36, 37]. While classical risk factors such as age, hypertension, diabetes, smoking, sedentary lifestyle, and hyperlipidemia are well established [38, 39], recent evidence highlights sex-specific differences in coronary dysfunction. Notably, premenopausal women with excess breast gland adiposity – reflected by lower mammographic breast density – demonstrate higher long-term risk of major adverse cardiovascular events (MACE), suggesting that female-specific metabolic–vascular responses, including insulin resistance and endothelial dysfunction, may influence MI susceptibility even in the absence of overt diabetes [40]. These observations highlight the importance of considering sex-specific mechanisms when developing MI biomarkers, such as *Slc6a4*, and when interpreting pathways that intersect with metabolic and endothelial homeostasis [3, 5, 39].

Our study highlights *Slc6a4* as a potential key mediator in MI. *Slc6a4* encodes the serotonin transporter, a protein that plays a crucial role in neurotransmission and cardiovascular regulation. Previous studies link *Slc6a4* polymorphisms to increased MI risk, likely via serotonin-mediated effects on platelet activation or smooth muscle cell proliferation [41, 42]. Furthermore, platelet microparticle number is elevated in acute MI, correlating with the extent of myocardial damage [43]. These findings suggest that *Slc6a4* may influence not only myocardial injury but also broader cardiovascular pathologies, such as cerebrovascular disease and pulmonary hypertension.

At the cellular level, dysregulation of the cell cycle and apoptosis is central to myocardial injury [44–46]. Local anesthetics such as ropivacaine can induce cardiomyocyte toxicity, including cell cycle arrest and apoptosis, with the effect being less pronounced than bupivacaine [47]. Metallothionein has been shown to mitigate ropivacaine-induced apoptosis and energy disruption in isolated rabbit cardiomyocytes [48]. Additionally, local anesthetics can inhibit cancer cell proliferation and enhance chemotherapy-induced apoptosis through oxidative stress-related pathways [49]. In our study, ropivacaine induced G1-phase arrest and apoptosis in H9c2 cells, with a concentration of 2 mM eliciting the most significant effects. While this concentration exceeds typical plasma levels (2–11 μM), it is consistent with local tissue exposure in confined microenvironments and serves as a valid model for assessing cytotoxicity under hypoxic conditions [23].

Oxidative stress is a critical mechanism in MI pathophysiology, resulting from an imbalance between ROS production and antioxidant defenses [50–53]. Increased ROS, MDA, and LDH, alongside decreased SOD and ATP, indicate cellular injury [52–54]. Studies have demonstrated that modulation of oxidative stress, such as through dioscin or metallothionein, can reduce myocardial damage [48, 55]. Consistent with these findings, ropivacaine induced oxidative stress in H9c2 cells in our study, supporting the relevance of antioxidant mechanisms in cardiomyocyte protection.

The H/R model effectively simulates ischemia-reperfusion injury, allowing investigation of molecular mechanisms. Our findings suggest that *Slc6a4* silencing enhances Nrf2 nuclear translocation while inhibiting NLRP3 inflammasome activation, thereby reducing oxidative stress and apoptosis [32, 56–58]. Nrf2 is a key transcription factor mediating cellular antioxidant responses, and its activation suppresses NLRP3-mediated inflammatory damage [57]. These results indicate that *Slc6a4* may act upstream of the Nrf2/NLRP3 axis, linking serotonin transport to cardiomyocyte resilience under stress.

Dose-response analysis revealed that ropivacaine induced G1-phase arrest, oxidative stress, and apoptosis in a concentration-dependent manner, with *Slc6a4* silencing attenuating these effects, particularly at 2 mM. This suggests a potential cardioprotective role for *Slc6a4* modulation through regulation of the cell cycle and antioxidants. Clinical evidence supports integrating molecular insights with therapeutic strategies; for example, *SGLT2* inhibitors reduce ischemia-reperfusion injury and in-stent restenosis in diabetic MI patients independent of glycemic control [59, 60].

The regulation of Nrf2 by *SLC6A4* may involve multiple signaling pathways, including activation of upstream kinases (PI3K/Akt, ERK, p38 MAPK) via intracellular redox states, Keap1 dissociation, or serotonin-mediated modulation of Nrf2 nuclear translocation [24, 53, 61, 62]. Further studies are needed to clarify these mechanisms and their contribution to cardioprotection.

This study elucidated the protective role of *Slc6a4* in ropivacaine-induced cardiomyocyte injury, highlighting its regulatory effects on oxidative stress, apoptosis, and activation of the NLRP3 inflammasome. Nevertheless, several limitations should be acknowledged, and future investigations are warranted to strengthen the translational relevance of our findings. First, our conclusions are primarily based on *in vitro* experiments using the H9c2 cell line. While this rat embryonic cardiomyoblast model provides valuable insights, it

differs from adult cardiomyocytes in terms of their electrophysiological properties, metabolic profiles, and responses to stress stimuli. To address this limitation, future studies will incorporate primary adult cardiomyocytes and animal models of MI, employing *Slc6a4* knockdown or overexpression, followed by a comprehensive assessment of cardiac function, histopathological changes, and systemic responses. Second, the clinical expression profile and significance of *Slc6a4* remain uncharacterized. Future work will focus on analyzing *Slc6a4* expression in myocardial tissues from MI patients using qRT-PCR and immunohistochemistry, and correlating these data with clinical parameters such as infarct size, cardiac biomarkers, and inflammatory mediators, to evaluate its diagnostic and prognostic potential. Third, additional candidate genes identified in the bioinformatics analysis, including *PCSK2* and *POMC*, require functional validation. Subsequent research will involve siRNA-mediated knockdown or overexpression of these genes in cardiomyocytes, coupled with pathway enrichment analyses (e.g., GO, KEGG) to delineate their involvement in relevant signaling networks. Finally, to enhance clinical translation, future studies will investigate intervention strategies targeting the *Slc6a4* gene. Potential approaches include screening small molecule agonists or inhibitors, applying RNA interference or gene editing technologies, and assessing the safety and efficacy of candidate therapies in animal models. Moreover, targeted drug delivery systems, such as nanocarriers, may improve myocardial specificity. The therapeutic potential of *Slc6a4* will also be evaluated in other disease models, such as acute liver injury and infectious conditions, as well as in preclinical trials. Collectively, these studies will deepen the understanding of *Slc6a4*'s role in MI and provide a foundation for its development as a therapeutic target and clinical biomarker.

In conclusion, our study effectively delineates the protective roles of *Slc6a4* in mitigating ropivacaine-induced cytotoxic effects under HR conditions in H9c2 cells. We demonstrated that ropivacaine exposure leads to cell cycle arrest, apoptosis, and oxidative stress by modulating the expression and activity of key cellular biomarkers. These novel findings highlight the potential of *Slc6a4* as a therapeutic target for myocardial ischemia-reperfusion injury. Notably, *Slc6a4* knockdown emerged as a pivotal modulator, attenuating the detrimental effects of ropivacaine by regulating the NLRP3 inflammasome and Nrf2 pathways. The downregulation of inflammasome-related proteins and the enhanced nuclear translocation of Nrf2 in *Slc6a4*-silenced cells suggest that this gene may play a crucial role in mitigating inflammatory responses and cell death. These findings highlight the potential of *Slc6a4* as a target for cardioprotective therapies in clinical settings, proposing new avenues for treatment development against cardiac pathologies induced by local anesthetics.

Acknowledgments

Jing Wan and Xiaonan Du contributed equally.

Funding

No external funding.

Ethical approval

Not applicable.

Conflict of interest

The authors declare no conflict of interest.

References

1. Upadhyay RK. High cholesterol disorders, myocardial infarction and its therapeutics. World J Cardiovasc Dis 2023; 13: 433-69.
2. Ambroziak M, Niewczas-Wieprzowska K, Maicka A, Budaj A. Younger age of patients with myocardial infarction is associated with a higher number of relatives with a history of premature atherosclerosis. BMC Cardiovasc Disord 2020; 20: 410.
3. Libby P, Ridker PM, Hansson GK. Inflammation in atherosclerosis: from pathophysiology to practice. J Am Coll Cardiol 2009; 54: 2129-38.
4. Messerli FH, Rimoldi SF, Bangalore S. The transition from hypertension to heart failure: contemporary update. JACC Heart Fail 2017; 5: 543-51.
5. Low Wang CC, Hess CN, Hiatt WR, Goldfine AB. Clinical update: cardiovascular disease in diabetes mellitus: atherosclerotic cardiovascular disease and heart failure in type 2 diabetes mellitus - mechanisms, management, and clinical considerations. Circulation 2016; 133: 2459-502.
6. Sardu C, Paolisso G, Marfella R. Inflammatory related cardiovascular diseases: from molecular mechanisms to therapeutic targets. Curr Pharm Des 2020; 26: 2565-73.
7. Sardu C, Massetti M, Testa N, et al. Effects of sodium-glucose transporter 2 inhibitors (SGLT2-I) in patients with ischemic heart disease (IHD) treated by coronary artery bypass grafting via MiECC: inflammatory burden, and clinical outcomes at 5 years of follow-up. Front Pharmacol 2021; 12: 777083.
8. Sardu C, D'Onofrio N, Torella M, et al. Metformin therapy effects on the expression of sodium-glucose cotransporter 2, leptin, and SIRT6 levels in pericoronary fat excised from pre-diabetic patients with acute myocardial infarction. Biomedicines 2021; 9: 904.
9. Marfella R, Prattichizzo F, Sardu C, et al. Evidence of an anti-inflammatory effect of PCSK9 inhibitors within the human atherosclerotic plaque. Atherosclerosis 2023; 378: 117180.
10. Ambrose JA, Barua RS. The pathophysiology of cigarette smoking and cardiovascular disease: an update. J Am Coll Cardiol 2004; 43: 1731-7.
11. Kumar Singh A, Kumar Jat R. Myocardial infarction. Himalayan J Health Sci 2022; 6: 16-32.

12. Ibanez B, James S, Agewall S, et al. 2017 ESC Guidelines for the management of acute myocardial infarction in patients presenting with ST-segment elevation. Kardiol Pol 2018; 76: 229-313.
13. Anderson JL, Morrow DA. Acute myocardial infarction. N Engl J Med 2017; 376: 2053-64.
14. Stevens JR, Zamani A, Osborne JIA, Zamani R, Akrami M. Critical evaluation of stents in coronary angioplasty: a systematic review. Biomed Engineering Online 2021; 20: 46.
15. Satish S. Advancements in pharmacotherapy for myocardial infarction: a comprehensive review. Int J Pharm Sci 2023; 1: 534.
16. Jankovic D. Regional nerve block in anesthesia and pain therapy: general consideration. In: Regional Nerve Blocks in Anesthesia and Pain Therapy: Imaging-guided and Traditional Techniques. Jankovic D, Peng P (eds.). Springer International Publishing, Cham 2022; 3-31.
17. Jin Z, Liu J, Li R, Gan TJ, He Y, Lin J. Single injection Quadratus Lumborum block for postoperative analgesia in adult surgical population: a systematic review and meta-analysis. J Clin Anesth 2020; 62: 109715.
18. McClure JH. Ropivacaine. Br J Anaesth 1996; 76: 300-7.
19. Graf BM, Abraham I, Eberbach N, Kunst G, Stowe DF, Martin E. Differences in cardiotoxicity of bupivacaine and ropivacaine are the result of physicochemical and stereoselective properties. Anesthesiology 2002; 96: 1427-34.
20. Capdevila X, Pirat P, Bringuier S, et al. Continuous peripheral nerve blocks in hospital wards after orthopedic surgery: a multicenter prospective analysis of the quality of postoperative analgesia and complications in 1,416 patients. Anesthesiology 2005; 103: 1035-45.
21. Ilfeld BM. Continuous peripheral nerve blocks: a review of the published evidence. Anesth Analg 2011; 113: 904-25.
22. Martínez-Martínez E, Ibarrola J, Fernández-Celis A, et al. Differential proteomics identifies reticulocalbin-3 as a novel negative mediator of collagen production in human cardiac fibroblasts. Sci Rep 2017; 7: 12192.
23. Zeng L, Li A, Zhang Z, et al. Ropivacaine induces cell cycle arrest in the G0/G1 phase and apoptosis of PC12 cells via inhibiting mitochondrial STAT3 translocation. Inflammation 2021; 44: 2362-76.
24. Zhang W, Shi C, Yao Z, Qian S. Bardoxolone methyl attenuates doxorubicin-induced cardiotoxicity by inhibiting the TXNIP-NLRP3 pathway through Nrf2 activation. Environ Toxicol 2024; 39: 1936-50.
25. Tong R, Jia T, Shi R, Yan F. Inhibition of microRNA-15 protects H9c2 cells against CVB3-induced myocardial injury by targeting NLRX1 to regulate the NLRP3 inflammasome. Cell Mol Biol Lett 2020; 25: 6.
26. Xia W, Li Y, Wu M, et al. Gasdermin E deficiency attenuates acute kidney injury by inhibiting pyroptosis and inflammation. Cell Death Dis 2021; 12: 139.
27. Yang X, Chen D, Zheng S, et al. The Prmt5-Vasa module is essential for spermatogenesis in Bombyx mori. PLoS Genet 2023; 19: e1010600.
28. Valussi M, Besser J, Wystub-Lis K, et al. Repression of Osmr and Fgfr1 by miR-1/133a prevents cardiomyocyte dedifferentiation and cell cycle entry in the adult heart. Sci Adv 2021; 7: eabi6648.
29. Wang AJ, Tang Y, Zhang J, et al. Cardiac SIRT1 ameliorates doxorubicin-induced cardiotoxicity by targeting sestrin 2. Redox Biol 2022; 52: 102310.
30. Wang J, Xie SA, Li N, et al. Matrix stiffness exacerbates the proinflammatory responses of vascular smooth muscle cell through the DDR1-DNMT1 mechanotransduction axis. Bioact Mater 2022; 17: 406-24.
31. Wang L, Liu J, Wang Z, et al. Dexmedetomidine abates myocardial ischemia reperfusion injury through inhibition of pyroptosis via regulation of miR-665/MEF2D/Nrf2 axis. Biomed Pharmacother 2023; 165: 115255.
32. Li F, Zhu H, Chang Z, Li Y. Gentiopicroside alleviates acute myocardial infarction injury in rats by disrupting Nrf2/NLRP3 signaling. Exp Biol Med 2023; 248: 1254-66.
33. Zhang YM, Zhang ZY, Wang RX. Protective mechanisms of quercetin against myocardial ischemia reperfusion injury. Front Physiol 2020; 11: 506938.
34. Lin P, Cao J, Ren P, et al. Network pharmacology and experimental validation to explore mechanism of tetrahydropalmatine on acute myocardial ischemia. Chin J Integr Med 2023; 29: 1087-98.
35. Coto E, Reguero JR, Alvarez V, et al. 5-Hydroxytryptamine 5-HT2A receptor and 5-hydroxytryptamine transporter polymorphisms in acute myocardial infarction. Clin Sci 2003; 104: 241-5.
36. Bhatt DL, Lopes RD, Harrington RA. Diagnosis and treatment of acute coronary syndromes: a review. JAMA 2022; 327: 662-75.
37. Akşit E, Büyük B, Oğuz S. Histopathological changes in myocardial tissue due to coronary venous hypertension. Arch Med Sci 2023; 19: 1714-20.
38. Awasthi S, Chalapathy CV. BEYOND THE BEATS. A Comprehensive Guide to. LAP LAMBERT Academic Publishing 2023.
39. Bays HE, Taub PR, Epstein E, et al. Ten things to know about ten cardiovascular disease risk factors. Am J Prev Cardiol 2021; 5: 100149.
40. Sardu C, Gatta G, Pieretti G, et al. Pre-menopausal breast fat density might predict MACE during 10 years of follow-up: the BRECARD Study. JACC Cardiovasc Imaging 2021; 14: 426-38.
41. Fishbein GA, Fishbein MC, Wang J, Buja LM. Myocardial ischemia and its complications. In: Cardiovascular Pathology. Buja LM, Butany J (eds.). Elsevier 2022; 407-45.
42. Moyer AM, Walker DL, Avula R, et al. Relationship of genetic variation in the serotonin transporter gene (SLC6A4) and congenital and acquired cardiovascular diseases. Genet Test Mol Biomarkers 2015; 19: 115-23.
43. Hartopo AB, Puspitawati I, Gharini PP, Setianto BY. Platelet microparticle number is associated with the extent of myocardial damage in acute myocardial infarction. Arch Med Sci 2016; 12: 529-37.
44. Malumbres M. Control of the cell cycle. In: Abeloff's Clinical Oncology. Niederhuber JE, Armitage JO, Doroshow JH, et al. (eds.). Elsevier 2020; 56-73.
45. Hu XM, Zhang Q, Zhou RX, et al. Programmed cell death in stem cell-based therapy: mechanisms and clinical applications. World J Stem Cells 2021; 13: 386-415.
46. Luo X, Zhou J, Wang Z, et al. An inhibitor role of Nrf2 in the regulation of myocardial senescence and dysfunction after myocardial infarction. Life Sci 2020; 259: 118199.
47. Zink W, Bohl JR, Hacke N, Sinner B, Martin E, Graf BM. The long term myotoxic effects of bupivacaine and ropivacaine after continuous peripheral nerve blocks. Anesthesia Analgesia 2005; 101: 548-54.
48. Zhu Y, Yuan Z, Liu X, Jing G. Effect of metallothionein on myocyte apoptosis and energy supply of isolated rabbit heart muscle during perfusion with ropivacaine. Nan Fang Yi Ke Da Xue Xue Bao 2011; 31: 1425-7.
49. Zhu G, Zhang L, Dan J, Zhu Q. Differential effects and mechanisms of local anesthetics on esophageal carci-

noma cell migration, growth, survival and chemosensitivity. BMC Anesthesiol 2020; 20: 126.
50. Demirci-Cekic S, Özkan G, Avan AN, Uzunboy S, Çapanoğlu E, Apak R. Biomarkers of oxidative stress and antioxidant defense. J Pharm Biomed Analysis 2022; 209: 114477.
51. Martemucci G, Costagliola C, Mariano M, D'andrea L, Napolitano P, D'Alessandro AG. Free radical properties, source and targets, antioxidant consumption and health. Oxygen 2022; 2: 48-78.
52. Jelic MD, Mandic AD, Maricic SM, Srdjenovic BU. Oxidative stress and its role in cancer. J Cancer Res Ther 2021; 17: 22-8.
53. Saxena P, Selvaraj K, Khare SK, Chaudhary N. Superoxide dismutase as multipotent therapeutic antioxidant enzyme: role in human diseases. Biotechnol Letters 2022; 44: 1-22.
54. Zhu XA, Gao LF, Zhang ZG, Xiang DK. Down-regulation of miR-320 exerts protective effects on myocardial IR injury via facilitating Nrf2 expression. Eur Rev Med Pharmacol Sci 2019; 23: 1730-41.
55. Zhang Z, Zhao X, Gao M, et al. Dioscin alleviates myocardial infarction injury via regulating BMP4/NOX1-mediated oxidative stress and inflammation. Phytomedicine 2022; 103: 154222.
56. Zhang W, Shi C, Yao Z, Qian S. Bardoxolone methyl attenuates doxorubicin-induced cardiotoxicity by inhibiting the TXNIP–NLRP3 pathway through Nrf2 activation. Environ Toxicol 2024; 39: 1936-50.
57. Zhang Q, Wang L, Wang S, et al. Signaling pathways and targeted therapy for myocardial infarction. Signal Transd Targeted Ther 2022; 7: 78.
58. Fan ZX, Yang CJ, Li YH, Yang J, Huang CX. Ginsenoside Rh2 attenuates myocardial ischaemia-reperfusion injury by regulating the Nrf2/HO-1/NLRP3 signalling pathway. Exp Ther Med 2023; 25: 35.
59. Marfella R, Sardu C, D'Onofrio N, et al. SGLT-2 inhibitors and in-stent restenosis-related events after acute myocardial infarction: an observational study in patients with type 2 diabetes. BMC Med 2023; 21: 71.
60. Paolisso P, Bergamaschi L, Cesaro A, et al. Impact of SGLT2-inhibitors on contrast-induced acute kidney injury in diabetic patients with acute myocardial infarction with and without chronic kidney disease: insight from SGLT2-I AMI PROTECT registry. Diabetes Res Clin Pract 2023; 202: 110766.
61. Rahim I, Sayed RK, Fernández-Ortiz M, et al. Melatonin alleviates sepsis-induced heart injury through activating the Nrf2 pathway and inhibiting the NLRP3 inflammasome. Naunyn-Schmiedeberg's Arch Pharmacol 2021; 394: 261-77.
62. Gurbanov R, Kalkanci B. SLC6A4 (solute carrier family 6 member 4). Atlas Atlas Genet Cytogenet Oncol Haematol 2020; 24: 39-50.